Cerebral Cortex, June 2018;28: 2175–2191

doi: 10.1093/cercor/bhx123
Advance Access Publication Date: 19 May 2017
Original Article

ORIGINAL ARTICLE

A Schizophrenia-Related Deletion Leads to KCNQ2-Dependent Abnormal Dopaminergic Modulation of Prefrontal Cortical Interneuron Activity

Se Joon Choi[1], Jun Mukai[2,3], Mirna Kvajo[2,3], Bin Xu[3], Anastasia Diamantopoulou[2,3], Pothitos M. Pitychoutis[4], Bin Gou[5], Joseph A. Gogos[2,6] and Hui Zhang[1,3,5,7]

[1]Department of Neurology, Columbia University, New York, NY10032, USA, [2]Department of Physiology and Cellular Biophysics, Columbia University, New York, NY 10032, USA, [3]Department of Psychiatry, College of Physicians and Surgeons, Columbia University, New York, NY 10032, USA, [4]Department of Biology, Center for Tissue Regeneration and Engineering (TREND), University of Dayton, 300 College Park, Dayton, OH 45469, USA, [5]Department of Neuroscience, Thomas Jefferson University, Philadelphia, PA 19107, USA, [6]Department of Neuroscience, College of Physicians and Surgeons, Columbia University, New York, NY 10032, USA and [7]Current address: Department of Neuroscience, Thomas Jefferson University, Philadelphia, PA 19107, USA

Address correspondence to Joseph A. Gogos, Department of Physiology and Neuroscience, Columbia University, 650 W 168th Street, New York, NY 10032, USA. Email: jag90@cumc.columbia.edu; Hui Zhang, Department of Neuroscience, Thomas Jefferson University, Philadelphia, PA 19107, USA. Email: hui.x.zhang@jefferson.edu

Abstract

Altered prefrontal cortex function is implicated in schizophrenia (SCZ) pathophysiology and could arise from imbalance between excitation and inhibition (E/I) in local circuits. It remains unclear whether and how such imbalances relate to genetic etiologies. We used a mouse model of the SCZ-predisposing 22q11.2 deletion (*Df(16)A*$^{+/-}$ mice) to evaluate how this genetic lesion affects the excitability of layer V prefrontal pyramidal neurons and its modulation by dopamine (DA). *Df(16)A*$^{+/-}$ mice have normal balance between E/I at baseline but are unable to maintain it upon dopaminergic challenge. Specifically, in wild-type mice, D1 receptor (D1R) activation enhances excitability of layer V prefrontal pyramidal neurons and D2 receptor (D2R) activation reduces it. Whereas the excitatory effect upon D1R activation is enhanced in *Df(16)A*$^{+/-}$ mice, the inhibitory effect upon D2R activation is reduced. The latter is partly due to the inability of mutant mice to activate GABAergic parvalbumin (PV)+ interneurons through D2Rs. We further demonstrate that reduced KCNQ2 channel function in PV+ interneurons in *Df(16)A*$^{+/-}$ mice renders them less capable of inhibiting pyramidal neurons upon D2 modulation. Thus, DA modulation of PV+ interneurons and control of E/I are altered in *Df(16)A*$^{+/-}$ mice with a higher excitation and lower inhibition during dopaminergic modulation.

Key words: dopamine, interneuron, KCNQ, prefrontal cortex, schizophrenia

Introduction

The neurophysiological substrates of most psychiatric disorders are poorly understood. For psychiatric disorders with high heritability, such as schizophrenia (SCZ), accumulating information on genetic factors associated with disease-risk provides an accurate, unbiased and reliable route to pathophysiology (Arguello and Gogos 2011). One emerging principle of human genetic studies is that a range of diverse and seemingly unrelated genetic abnormalities can give rise to the same psychiatric phenotype (Rodriguez-Murillo et al. 2012). These findings unveil an exquisite sensitivity of the neural circuits underlying susceptibility to SCZ to precise levels or activity of many diverse proteins and signaling modules. They also highlight the need to understand how specific highly penetrant genetic lesions that can be readily modeled in mice affect the structure, function, and neuromodulation of neural circuits (Arguello and Gogos 2011; Karayiorgou et al. 2012; Crabtree and Gogos 2014).

SCZ is characterized by global abnormalities in brain function although some brain areas, circuits, and physiological processes may be more affected than others as indicated by the specific pattern of cognitive deficits and the highly unusual positive symptoms of the disease. Prefrontal cortex (PFC) function and connectivity in particular is implicated in SCZ by functional imaging studies indicating altered activation at baseline and during cognitive tests of PFC function. Whereas many studies report hypo-metabolism in the PFC of chronic medicated SCZ patients (Weinberger et al. 1986; Weinberger and Berman 1996), significantly higher regional glucose metabolism in frontal regions in drug-naïve and acutely psychotic patients with SCZ than in controls has also been reported (Cleghorn et al. 1989). PFC circuitry is also involved in executive function and working memory (WM) that are abnormal in SCZ. Indeed altered PFC function may impact upon multiple cognitive functions but also result in a more general susceptibility to psychopathology by failing to buffer disease effects on perception and affect (Manoach 2003; Barch and Ceaser 2012).

De novo hemizygous microdeletions of the chromosome 22q11.2 locus are one of the greatest genetic risk factors of SCZ. Carriers of these deletions exhibit a spectrum of cognitive deficits as children including deficits in WM and executive function and develop SCZ in adolescence or adulthood at a rate of 25–30% (Karayiorgou et al. 2010). Recurrent 22q11.2 deletions account for as many as 1–2% of cases of sporadic SCZ in the population and provide a leading example of the importance of rare mutations in psychiatric disorders and cognitive dysfunction. The majority of carriers have a 3-Mb deletion whereas 7% have a nested 1.5-Mb deletion that removes 27 known genes (Karayiorgou et al. 2010). To understand the molecular, cellular, and synaptic mechanisms underlying the cognitive dysfunction and psychiatric phenotypes associated with 22q11.2 deletions we have previously generated a mouse model carrying a 1.3-Mb chromosomal deficiency on chromosome 16, which is syntenic to the 22q11.2 1.5-Mb deletion [*Df(16)A*$^{+/-}$ mice] (Stark et al. 2008). At face value, *Df(16)A*$^{+/-}$ mice have shown features that parallel findings in individuals with SCZ, including deficits in prepulse inhibition, WM as well as well as neuroanatomical alterations both at the mesoscopic and microscopic level (Stark et al. 2008; Ellegood et al. 2014; Fenelon et al. 2013; Xu et al. 2013). Most importantly, analysis using a number of behavioral tests revealed a profile of cognitive deficits driven in part by a prominent effect of the mutation on PFC function and connectivity (Stark et al. 2008; Drew et al. 2011; Fenelon et al. 2011, 2013; Mukai et al. 2015). Consistent with the behavioral findings our previous analysis implicated altered structure and function of PFC circuitry in the *Df(16)A*$^{+/-}$ mice (Fenelon et al. 2011, 2013; Mukai et al. 2015).

Dysfunction of local PFC circuits in patients and genetic animal models can arise in part due to global or finer-scale changes in excitation and inhibition (E/I) balance (Marin 2012). It has been shown, for example, that optogenetic perturbation leading to alterations in this balance in PFC microcircuitry could give rise to social and cognitive deficits in mice (Yizhar et al. 2011). However, such wholesale perturbations only partially capture disease-related circuit dysfunction, as they do not take into consideration neuromodulatory influences that may affect specific aspects of excitatory or inhibitory transmission and the coordination between pyramidal and GABAergic interneurons, leading to finer-scale E/I circuit imbalances, evident only under specific conditions (Crabtree et al. 2016). Moreover, there is an extensive literature indicating abnormalities consistent with reduced interneuron activity, mainly of parvalbumin (PV) containing interneurons, in brains of individuals with SCZ. Data from such human postmortem studies are limited by methodological issues and could be interpreted as supportive of either a primary deficit or a secondary/compensatory effect to reduced excitatory transmission (Hoftman et al. 2016). Such studies have also limitations because they do not take into consideration the high genetic heterogeneity of the disease. Overall, while altered PV+ interneuron activity very likely contributes to the circuit alterations emerging as a result of many SCZ risk mutations, its role is likely complicated and possible mutation-specific and cannot be adequately described in terms of a simple hyper- or hypo-activity context. Nevertheless, whether 22q11.2 deletions or any other genuine SCZ-predisposing mutation lead to E/I imbalances in the PFC and the ensuing pattern of cellular dysfunction remains unknown.

Here, we show that *Df(16)A*$^{+/-}$ mice have normal excitation–inhibition at baseline but are unable to maintain normal balance upon dopaminergic challenge. In wild-type (WT) mice, dopamine (DA) D1 receptor (D1R) activation enhances excitability of layer V prefrontal pyramidal neurons and D2 receptor (D2R) activation reduces it. Whereas the excitatory effect on the excitability of layer V prefrontal pyramidal neurons upon D1R activation is enhanced in *Df(16)A*$^{+/-}$ mice, the inhibitory effect upon D2R activation is reduced. We also show that the latter is partly due to the inability of mutant mice to activate GABAergic PV+ interneurons through D2Rs. We further demonstrate a previously unknown role of the KCNQ channels in mediating the abnormal neuromodulation by D2Rs. Impaired KCNQ-channel function in the PV+ interneurons of *Df(16)A*$^{+/-}$ mice renders these neurons less capable of inhibiting pyramidal cells upon D2R modulation. Thus, the DA modulation of PV+ interneurons and coordination between pyramidal and GABAergic interneurons is altered in *Df(16)A*$^{+/-}$ mice with a higher excitation and lower inhibition than WT mice during DA challenge.

Materials and Methods

Animals and Slice Preparation

The use of the animals followed the National Institutes of Health guidelines and was approved by the Institutional Animal Care and Use Committee of Columbia University and Thomas Jefferson University. Generation of *Df(16)A*$^{+/-}$ mice has been described previously (Stark et al. 2008). *Df(16)A*$^{+/-}$ mice have been backcrossed into C57BL/6J background for over

10 generations. To visualize PV+ interneurons, *Df(16)A*$^{+/-}$ mice were crossed with GAD67-GFP mice (Chattopadhyaya et al. 2004, G42 mice obtained from The Jackson Laboratory) to generate *Df(16)A*$^{+/-}$; GAD67-GFP$^{+/-}$ and WT littermates in which PV+ interneurons are labeled by GFP.

Given that DA signaling in mPFC continues to mature during adolescence, we conducted all recordings in mPFC slices obtained from the post pubertal (8- to 12-wk-old) mice. Male mice were anesthetized with isoflurane before being decapitated. Coronal slices (300 μm) containing the mPFC were prepared using vibrotome (VT1200) in oxygenated ice cold modified-artificial cerebrospinal fluid (ACSF) containing (in mM) 125.2 NaCl, 26.2 $NaHCO_3$, 10 glucose, 2.5 KCl, 0.4 NaH_2PO_4, 0.4 KH_2PO_4, 0 $CaCl_2$, 3.7 $MgSO_4$, pH 7.40; osmolarity 290 ± 5 mOsm. Slices were incubated at 36 °C in oxygenated ACSF containing 2.4 mM $CaCl_2$ and 1.3 mM $MgSO_4$ for at least 1 h before recording.

Electrophysiology

Whole-cell patch-clamp recordings were performed on layers V–VI mPFC through an upright Olympus BX50WI (Olympus) differential interference contrast microscope with a 40× water immersion objective and an IR-sensitive video camera. All experiments were conducted at 35–36 °C. For the recording, slices were submerged in a flowing ACSF (2 mL/min). Pipettes (3–5 MΩ) were filled with (in mM): 115 K-gluconate, 10 HEPES, 2 $MgCl_2$, 20 KCl, 2 MgATP, 1 Na_2-ATP, 0.3 GTP, pH = 7.3; 280 ± 5 mOsm. Quinpirole, SKF 38393, sulpiride, SCH23390, and NMDA were purchased from Sigma and TTX, APV, CNQX, XE991, and TDZD were obtained from Tocris.

Whole-cell patch-clamp recordings were performed with a multiclamp 700B amplifier (Molecular Devices) and digitized at 10 kHz with a Digidata 1440 A (Molecular Devices). Data were acquired using Clampex 10.2 software (Molecular Devices) for subsequent analysis. In each cell, input resistance (measured by 100 pA, 100 ms duration hyperpolarizing pulses), membrane potential, the number of evoked spikes, and the latency to the first spike evoked by a 500 ms duration depolarizing current pulse (150–450 pA) were injected at 1 min interval and analyzed before and after drug treatment. To examine the effect on PFC pyramidal neuron excitability, current intensities were adjusted to evoke 2 spikes during baseline for drugs with known increase in cell excitability (e.g., D1 agonist, NMDA) or 4 spikes for drugs with known attenuation of cell excitability (e.g., quinpirole). For most of the figures, we chose to plot the normalized number of spikes to show the effect of a drug on the number of spikes (before and after drug application) and the development of change in spike numbers over time. The normalized number of spikes is in response to a single current step. Baseline recordings were conducted for 5 min after observing stabilized spike number and drugs were applied for 10–15 min. All comparisons with baseline conditions were conducted 6–10 min after the onset of drug application. The data in the last 5 min during drug application and the last 5 min of various control conditions were averaged respectively and compared. For experiments measuring KCNQ currents, cell were depolarized to −20 mV and then 500 ms duration of +10 mV voltage steps were delivered from −60 to −20 mV in the voltage clamp mode in the presence of 1 μM TTX. All the measurements with whole-cell mode were conducted within the first 30 min of the recordings. Gramicidin perorated patch-clamp recording was used to minimize intracellular dialysis for some of the experiments measuring KCNQ currents. About 100 μg/mL gramicidin was added to filling solution. Pipettes were front-filled with regular solution and back-filled with gramicidin-containing solution. A 200 mg/mL gramicidin stock solution was made fresh daily in DMSO and diluted to obtain the final concentration of the solvent to 0.05%. The perforated patch was considered as complete when the access resistance reaching 50 mΩ or less. Bridge balance was not corrected, but access resistance was periodically monitored and data were discarded if access resistance changed by more than 20% during an experiment.

For miniature excitatory postsynaptic currents (mEPSCs) experiments, whole-cell voltage clamp recording mode was performed in the presence of 1 μM TTX and 50 μM biccuculin. Pipette solution contained (in mM): 120 $CsMeSO_3$, 5 NaCl, 10 HEPES, 1.1 EGTA, 2 Mg^{2+}-ATP, 0.3 Na-GTP, 2 Na-ATP, 5 QX314, pH = 7.3; 280 ± 5 mOsm. For miniature inhibitory postsynaptic currents (mIPSCs) experiments, whole-cell voltage clamp recording mode was performed in the presence of 1 μM TTX, 50 μM APV, and 10 μM CNQX. Pipette solution contained high concentration of chloride to induce inward mIPSCs (in mM): 140 $CsCl_2$, 2 $MgCl_2$, 10 HEPES, 2 EGTA, 2 MgATP, 1 Na_2-ATP, 0.3 GTP, 5 QX314, pH = 7.3; 280 ± 5 mOsm. Recordings were run with gap-free protocol. Miniature events were detected and analyzed using Mini Analysis program (Synaptosoft). The threshold for amplitude detection of an event was generally adjusted to twice the RMS noise level (typically 8 pA). All data shown except mEPSCs, spontaneous excitatory postsynaptic current (sEPSCs), mIPSCs, and spontaneous IPSCs (sIPSCs) were analyzed with Clampfit 10.2 software (Molecular Devices).

Single Nucleotide Polymorphism Interaction Analysis

Single nucleotide polymorphism (SNP) interaction analysis used 8024 cases and 7798 controls from the Psychiatric GWAS Consortium (PGC) SCZ case/control data set. Genotypes of all SNPs within the KCNQ2 and DRD2 genomic regions were extracted using PLINK (Purcell et al. 2007). Pair-wise interaction analysis was conducted with PLINK-epistasis option (http://pngu.mgh.harvard.edu/~purcell/plink/epi.shtml). We conducted 10 000 permutations by shuffling the case/control labels with PLINK–permutation option and run epistasis with the same setting as the actual analysis. The outputs of permutation were combined and analyzed in the R package. The minimum *P*-value of each permutation was extracted and the *P*-values less than the observed minimum *P*-value were counted.

Total RNA Isolation and qRT-PCR, Immunohistochemistry, and Image Acquisition

See the Supplemental Experimental Procedures for details.

Data and Statistical Analysis

Data were expressed as mean ± SEM unless specified. Mann–Whitney test, Wilcoxon test, *t*-test, one-way, or two-way ANOVA followed by Bonferroni post-test was performed using Prism 7.0 (GraphPad). The difference was considered statistically significant when $P < 0.05$. Statistical analysis is based on number of cells or experiments unless specified. *N* stands for the number of mice and *n* stands for the number of experiments.

Results

Normal Excitability of Layer V Pyramidal Neurons in *Df(16)A*$^{+/-}$ Mice

To determine the impact of 22q11.2 microdeletion on PFC microcircuitry, we first used whole-cell current-clamp recordings to

examine the passive membrane and firing properties of layer V pyramidal neurons in prefrontal slices from adult *Df(16)A*$^{+/-}$ mice and WT littermates (P60-P90). All recordings were performed in deep layers of the medial PFC (mPFC, prelimbic, and infralimbic regions) with visual guidance and the identification of layer V pyramidal cells was based on their large soma size. Only one neuron per slice was recorded and usually 2–4 cells were obtained per animal. These neurons were silent at rest but showed action potential firing in response to depolarizing current pulses (Fig. 1*A*) and inward rectification with hyperpolarizing current injections (Fig. 1*B*). We found no alteration in the current–voltage (IV) relationship (Fig. 1*B*), and no difference in resting membrane potential (WT: −71.1 ± 0.5 mV, $n = 84$; *Df(16)A*$^{+/-}$: −70.8 ± 0.5 mV, $n = 84$, $P = 0.65$, *t*-test) and input resistance (WT: 183.7 ± 6.4 MΩ, $n = 62$; *Df(16)A*$^{+/-}$: 177.4 ± 6.1 MΩ, $n = 62$, $P = 0.25$, *t*-test). Moreover, there was no difference between WT and *Df(16)A*$^{+/-}$ neurons in the spike frequency in a range of depolarizing currents (Fig. 1*C*). Thus, excitability of layer V pyramidal neurons does not appear to be altered in adult *Df(16)A*$^{+/-}$ mice.

Excitability is influenced by the balance between excitatory and inhibitory synaptic inputs. Normal excitability of layer V pyramidal neurons of *Df(16)A*$^{+/-}$ mice suggests unaltered excitatory and inhibitory transmission balance at baseline. To test this, we compared the amplitude and frequency of sEPSCs and sIPSCs recorded from layer V mPFC pyramidal neurons of *Df(16)A*$^{+/-}$ mice and their WT littermates. Neither the amplitude (Fig. 1*E*) nor the frequency (Fig. 1*F*) of sEPSCs was different. Similarly, we found no difference in the amplitude and the frequency of sIPSCs (Fig. 1*G*,*H*). We further examined mEPSCs and mIPSCs, which are independent of action potentials and network activity, reflecting the number and strength of synapses but we did not detect any significant genotypic difference (Fig. 1*E*–*H*). Taken together, these results highlight a pattern of normal excitability of layer V pyramidal neurons as well as unaltered baseline excitatory and inhibitory synapse balance in *Df(16)A*$^{+/-}$ mice.

The Inhibitory Effect of D2R Activation on PFC Pyramidal Neuron Excitability is Reduced and the Excitatory Effect of D1R Activation of PFC Pyramidal Neuron Excitability is Enhanced in *Df(16)A*$^{+/-}$ Mice

DA modulates fast excitatory and inhibitory synaptic transmission in several brain regions. The PFC receives dopaminergic input from ventral tegmental area, and DA has been shown to modulate PFC circuits (Gao and Goldman-Rakic 2003; Tseng and O'Donnell 2004; Durstewitz and Seamans 2008; Tseng et al. 2008). To determine whether the mouse equivalent of the 22q11.2 microdeletion disrupts dopaminergic actions in the PFC, we assessed the dopaminergic modulation of pyramidal cell excitability by measuring the number of spikes and the latency to the first spike evoked by constant-amplitude depolarizing current pulses in slices from adult WT and *Df(16)A*$^{+/-}$ mice. We first examined the modulation effect by D2Rs since experiments in rat brain slices have shown that activation of D2Rs attenuates layer V pyramidal neuron excitability (Tseng and O'Donnell 2004) and recordings in vivo have shown that DA inhibits spontaneous and evoked firing of PFC neurons (Sesack and Bunney 1989) through D2Rs. In addition, the expression of D2Rs is restricted to layer V in comparison with a wider expression of D1Rs (Santana et al. 2009). Bath application of the D2 agonist quinpirole induced a concentration-dependent decrease of pyramidal cell excitability in both WT and *Df(16)A*$^{+/-}$ (Fig. 2*A*–*C*) without apparent changes in the membrane potential and input resistance (see Supplementary Fig. S1A and S1B). However, the inhibitory action of quinpirole on layer V pyramidal neurons was attenuated in *Df(16)A*$^{+/-}$ mice with the dose-response curve shifted to the right (Fig. 2*B*). In WT mice, 1 μM quinpirole decreased the number of evoked spikes from 4.0 ± 0.0 to 1.9 ± 0.5 ($P < 0.01$) and increased the latency to the first spike from 71.5 ± 4.4 ms to 103.0 ± 12.9 ($P < 0.05$). The same concentration of quinpirole failed to modify pyramidal neuron excitability in *Df(16)A*$^{+/-}$ mice. Increasing quinpirole concentration to 2 μM yielded a slight but statistically significant inhibitory effect. The inhibitory action of quinpirole on pyramidal cell excitability was completely blocked by 10 μM sulpiride (see Supplementary Fig. S1C) confirming that quinpirole-induced excitability decrease was D2R dependent.

The inhibitory effect of quinpriole appears to be layer-specific since application of quinpirole in layer II/III pyramidal neurons in WT mice slightly increases their firing (see Supplementary Fig. S2, ~22% increase).

For comparison, we also investigated the impact of D1Rs on local excitatory synaptic transmission in adult PFC pyramidal neurons. Bath application of the D1R agonist SKF38393 induced a concentration-dependent increase of pyramidal cell excitability in both WT and *Df(16)A*$^{+/-}$ mice (Fig. 2*D*–*F*) without apparent changes in the membrane potential and input resistance (see Supplementary Fig. S1D, S1E). However, the excitatory action of SKF38393 was enhanced in *Df(16)A*$^{+/-}$ mice with a dose-response curve shifted to the left (Fig. 2*E*).

Finally, recent studies suggest that PFC layer V pyramidal neurons can be divided into at least 2 subpopulations, 1 directly modulated by D1Rs and the other by D2Rs (Seong and Carter 2012), with different downstream targets and electrophysiological properties such as voltage sag in response to hyperpolarizing current (Dembrow et al. 2010). Whereas we observed 2 types of pyramidal neurons in PFC layer V (i.e., sag neurons and nonsag neurons) in both WT and *Df(16)A*$^{+/-}$ mice (see Supplementary Fig. S3A), the excitability of both sag and nonsag neurons in WT mice was decreased by D2R activation with sag neurons exhibiting higher sensitivity. Importantly, the inhibitory effect of D2R activation on pyramidal neuron excitability was greatly reduced in both sag and nonsag neurons from *Df(16)A*$^{+/-}$ mice (see Supplementary Fig. S3B). Regarding D1R action, there was no difference in the excitatory effect of SKF3839 on the excitability of both sag and nonsag neurons. Moreover, both sag and nonsag neurons from *Df(16)A*$^{+/-}$ mice showed enhanced excitability compared with WT mice upon D1R activation (see Supplementary Fig. S3C). Overall, the differences in D1R- or D2R- modulation on pyramidal neurons excitability between WT and *Df(16)A*$^{+/-}$ mice are not dependent on the neuronal subtype.

D2R-Mediated Inhibition of the Excitatory Effect of NMDA on PFC Pyramidal Neurons is Reduced in *Df(16)A*$^{+/-}$ Mice

Optimal interaction of DA-glutamate is required for PFC function (Durstewitz and Seamans 2008). We, therefore, examined whether 22q11.2 microdeletion affects the excitatory effect of NMDA on PFC pyramidal neurons and whether the interaction of NMDA-DA is altered. Bath application of NMDA elicited a

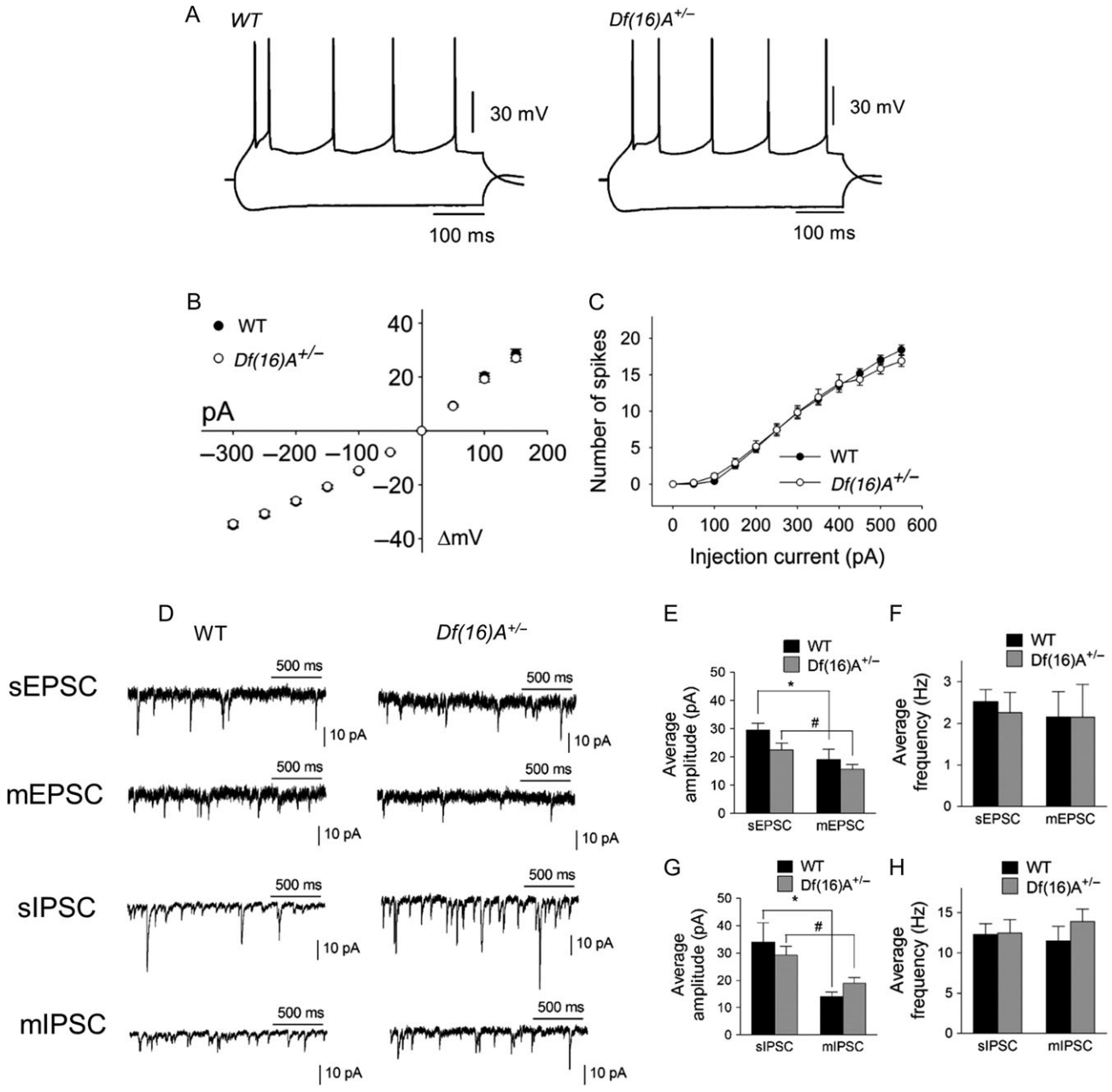

Figure 1. Whole-cell recordings of PFC layer V pyramidal neurons from WT and *Df(16)A*$^{+/-}$ mice show normal excitability and synaptic transmissions. (*A*) Representative traces of voltage responses to depolarizing and hyperpolarizing somatic current injection (−300 and +150 pA) from WT (top left) and *Df(16)A*$^{+/-}$ (top right) mice. (*B*) IV plot obtained from the traces shown in (*A*) for WT ($N = 41$, $n = 122$) and *Df(16)A*$^{+/-}$ ($N = 37$, $n = 111$) mice, $P = 0.84$, two-way ANOVA. (*C*) Comparison of excitability of pyramidal neurons from WT ($N = 8$, $n = 27$) and *Df(16)A*$^{+/-}$ ($N = 9$, $n = 27$) mice by depolarizing step currents (0 to + 550 pA, + 50 pA increment), $P = 0.66$, two-way ANOVA. (*D*) Representative traces of spontaneous and miniature EPSCs and IPSCs (sEPSC/sIPSC and mEPSC/mIPSC). (*E*) No difference in the average amplitude of sEPSCs or mEPSCs between WT and *Df(16)A*$^{+/-}$ mice was observed. sEPSC: WT, 29.6 ± 2.3 pA, $N = 3$, $n = 7$; *Df(16)A*$^{+/-}$, 22.5 ± 2.5 pA, $N = 3$, $n = 8$, $P = 0.07$. mEPSC: WT, 19.1 ± 3.5 pA, $n = 9$; *Df(16)A*$^{+/-}$ 15.6 ± 1.8 pA, $n = 8$, $P = 0.41$, Mann–Whitney test. (*F*) No change in the average frequency of sEPSCs or mEPSCs between WT and *Df(16)A*$^{+/-}$ mice was observed. sEPSC: WT, 2.5 ± 0.3 Hz, $n = 7$; *Df(16)A*$^{+/-}$, 2.3 ± 0.5 H, $n = 8$, $P = 0.66$. mEPSC: WT, 2.2 ± 0.6 Hz, $n = 9$; *Df(16)A*$^{+/-}$, 2.1 ± 0.8 Hz, $n = 8$, $P = 0.99$, Mann–Whitney test. (*G*) No difference in the average amplitude of sIPSCs or mIPSCs between WT and *Df(16)A*$^{+/-}$ mice was observed. sIPSC: WT, 34.0 ± 7.0 pA, $N = 4$, $n = 11$; *Df(16)A*$^{+/-}$, 29.3 ± 3.2 pA, $N = 4$, $n = 13$, $P = 0.84$. mIPSC: WT, 14.0 ± 1.8 pA, $n = 11$; *Df(16)A*$^{+/-}$, 18.9 ± 2.2 pA, $n = 11$, $P = 0.09$, Mann–Whitney test. (*H*) No change in the average frequency of sIPSCs or mIPSCs between WT and *Df(16)A*$^{+/-}$ mice was observed. sIPSC: WT, 12.3 ± 1.4 Hz, $n = 11$; *Df(16)A*$^{+/-}$, 12.5 ± 1.6 Hz, $n = 13$, $P = 0.89$. mIPSC: WT, 11.5 ± 1.8 Hz, $n = 11$; *Df(16)A*$^{+/-}$; 13.9 ± 1.5 Hz, $n = 11$, $P = 0.15$, Mann–Whitney test. The average amplitude of sEPSCs and sIPSCs was significantly decreased compared with mEPSCs and mIPSCs respectively. Data are shown as mean ± SEM. $^{*}P < 0.05$, $^{\#}P < 0.05$, $^{**}P < 0.01$.

dose-dependent increase in excitability in pyramidal neurons in WT (Fig. 3A–C), consistent with previous studies in rats (Tseng and O'Donnell 2004). However, in contrast to altered dopaminergic modulation of the excitability of PFC pyramidal neurons, we observed no significant difference of excitatory effect of NMDA on pyramidal neurons in WT and *Df(16)A*$^{+/-}$ mice (Fig. 3A–C). 4 μM NMDA increased the number of spikes in WT and *Df(16)A*$^{+/-}$. Bath application of 0.8 μM quinpirole

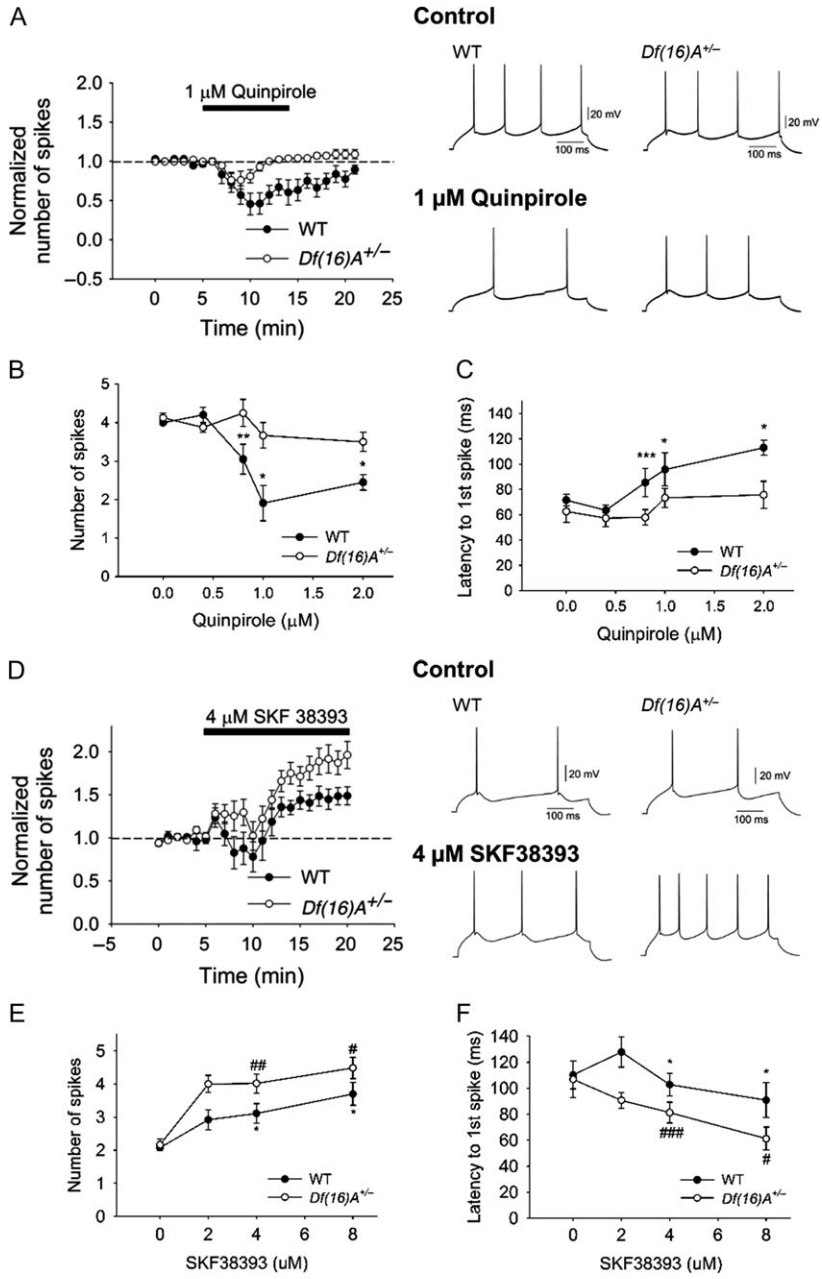

Figure 2. The inhibitory effect of D2R activation of PFC pyramidal neuron excitability is reduced whereas the excitatory effect of D1R activation of PFC pyramidal neuron excitability is enhanced in *Df(16)A*$^{+/-}$ mice. (*A*) Bath application of 1 μM quinpirole-induced greater decrease in the cell excitability in WT ($N = 7$, $n = 8$, $P = 0.014$, Wilcoxon test) than *Df(16)A*$^{+/-}$ ($N = 7$, $n = 10$, Wilcoxon test, $P = 0.10$) mice. Right panel illustrates the effect of quinpirole on the action potential firing induced by depolarizing current injection (150–250 pA) in single neurons from WT and *Df(16)A*$^{+/-}$ mice. (*B*) Quinpirole decreased cell excitability in a dose-dependent manner (0, 0.4, 0.8, 1.0, and 2.0 μM) in WT mice (before and after quinpirole, 0 μM: $N = 3$, $n = 4$, $P = 0.50$; 0.4 μM: $N = 3$, $n = 4$, $P = 0.25$; 0.8 μM: $N = 7$, $n = 14$, $P = 0.004$; 1 μM: $N = 7$, $n = 8$, $P = 0.014$; 2 μM: $N = 5$, $n = 5$, $P = 0.04$, Wilcoxon test) but led to significantly less decrease in *Df(16)A*$^{+/-}$ mice (before and after quinpirole, 0 μM: $N = 3$, $n = 4$, $P = 0.41$; 0.4 μM: $N = 3$, $n = 4$, $P = 1.00$; 0.8 μM: $N = 7$, $n = 11$, $P = 0.17$; 1 μM: $N = 7$, $n = 10$, $P = 0.10$; 2 μM: $N = 3$, $n = 6$, $P = 0.84$, Wilcoxon test; WT vs. *Df(16)A*$^{+/-}$: $P = 0.017$, two-way ANOVA). (*C*) Dose-dependent increase in first spike latency in WT mice (before and after quinpirole, 0 μM: $n = 4$, $P = 0.63$; 0.4 μM: $n = 4$, $P = 0.25$; 0.8 μM: $n = 14$, $P = 0.0004$; 1 μM: $n = 8$, $P = 0.02$; 2 μM: $n = 5$, $P = 0.03$, Wilcoxon test) was greater than *Df(16)A*$^{+/-}$ mice (before and after quinpirole, 0 μM: $n = 4$, $P = 0.50$; 0.4 μM: $n = 4$, $P = 0.63$; 0.8 μM: $n = 11$, $P = 0.30$; 1 μM: $n = 10$, $P = 0.16$; 2 μM: $n = 6$, $P = 0.31$; WT vs. *Df(16)A*$^{+/-}$: $P = 0.02$, two-way ANOVA). (*D*) Bath application of 4 μM SKF38393 induced less increase in cell excitability in WT ($N = 8$, $n = 9$, $P = 0.04$, Wilcoxon test) than in *Df(16)A*$^{+/-}$ mice ($N = 8$, $n = 12$, $P = 0.0023$, Wilcoxon test) mice. Right panel illustrates the effect of SKF38393 on the action potential firing induced by depolarizing current injection (100–150 pA) in single neurons from WT and *Df(16)A*$^{+/-}$ mice. (*E*) SKF38393 increased cell excitability in a dose-dependent manner (0, 2, 4, and 8 μM) in WT mice (before and after SKF38393, 0 μM: $N = 3$, $n = 4$, $P = 0.59$; 2 μM: $N = 4$, $n = 5$, $P = 0.13$; 4 μM: $N = 8$, $n = 9$, $P = 0.04$; 8 μM: $N = 3$, $n = 5$, $P = 0.03$, Wilcoxon test) but showed significantly greater increase in *Df(16)A*$^{+/-}$ mice (0 μM: $N = 3$, $n = 4$, $P = 0.57$; 2 μM: $N = 3$, $n = 5$, $P = 0.06$; 4 μM: $N = 8$, $n = 12$, $P = 0.0023$; 8 μM: $N = 3$, $n = 5$, $P = 0.02$, Wilcoxon test; WT versus *Df(16)A*$^{+/-}$: $P = 0.008$, two-way ANOVA). (*F*) Dose-dependent decrease in first spike latency in *Df(16)A*$^{+/-}$ mice (before and after SKF38393, 0 μM: $n = 4$, $P = 0.75$; 2 μM: $n = 5$, $P = 0.13$; 4 μM: $N = 8$, $n = 12$, $P = 0.0005$; 8 μM: $n = 5$, $P = 0.023$, Wilcoxon test) was greater than in WT mice (0 μM: $n = 4$, $P = 0.13$; 2 μM: $n = 5$, $P = 0.13$; 4 μM: $n = 9$, $P = 0.03$; 8 μM: $n = 5$, $P = 0.03$, Wilcoxon test; WT versus *Df(16)A*$^{+/-}$: $P = 0.005$, two-way ANOVA). Data are shown as mean ± SEM. $^{*}P < 0.05$, $^{\#}P < 0.05$, $^{**}P < 0.01$, $^{\#\#}P < 0.01$, $^{***}P < 0.001$, $^{\#\#\#}P < 0.001$.

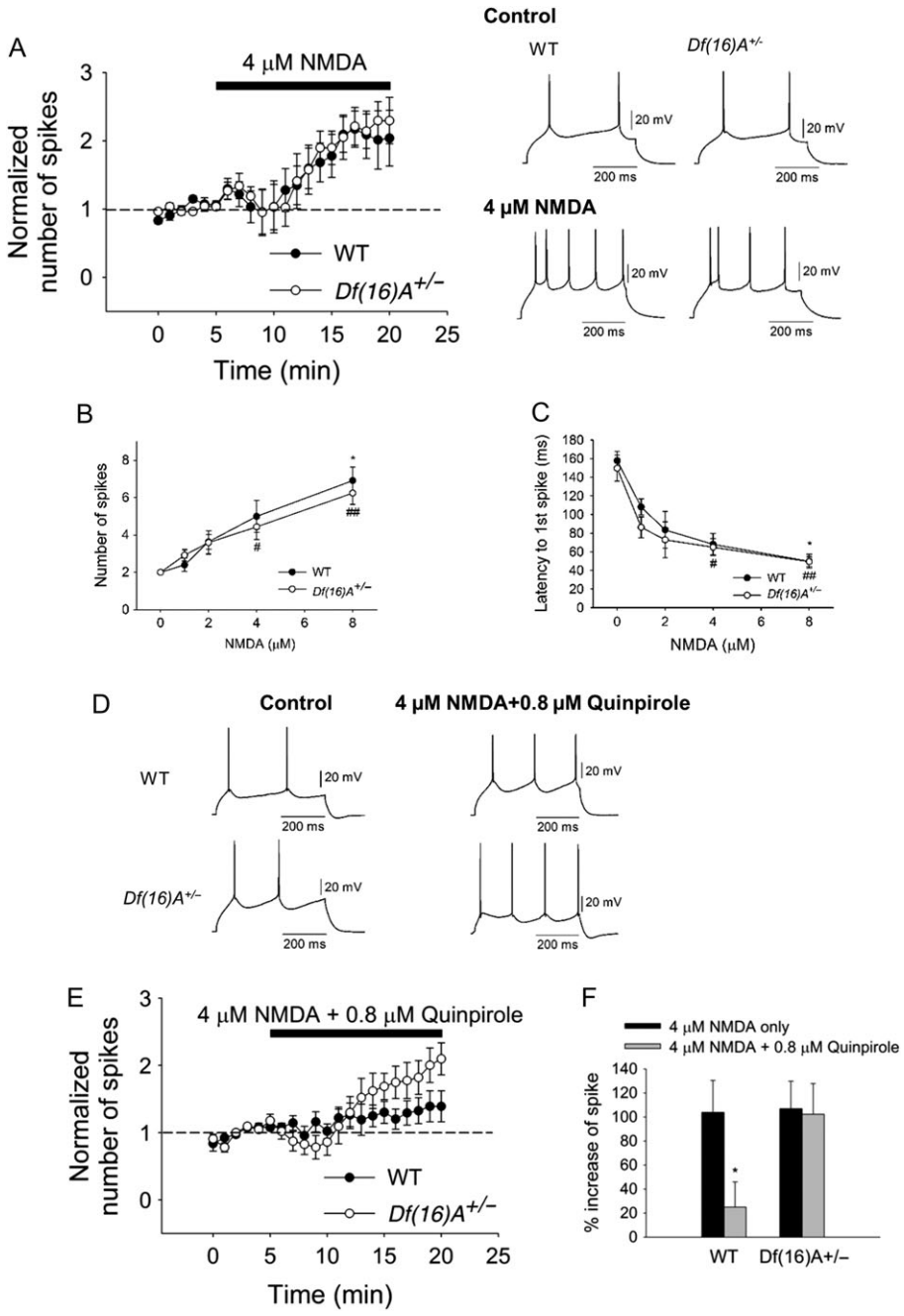

Figure 3. Inhibition of the excitatory effect of NMDA by D2R activation on PFC pyramidal neurons. (*A*) No significant difference in pyramidal neuron excitability between WT ($N = 3$, $n = 5$, $P = 0.06$, Wilcoxon test,) and *Df(16)A*$^{+/-}$ mice ($N = 4$, $n = 6$, $P = 0.03$, Wilcoxon test,) by bath application of 4 μM NMDA. (*B*) NMDA increased excitability in a dose-dependent manner (0, 1, 2, 4, and 8 μM) in WT mice (before and after NMDA, 0 μM: $N = 3$, $n = 4$, $P = 0.60$; 1 μM: $N = 3$, $n = 4$, $P = 0.41$; 2 μM: $N = 4$, $n = 5$, $P = 0.06$; 4 μM: $N = 3$, $n = 5$, $P = 0.06$; 8 μM: $N = 5$, $n = 7$, $P = 0.02$, Wilcoxon test) as well as in *Df(16)A*$^{+/-}$ mice (0 μM: $N = 3$, $n = 4$, $P = 0.50$; 1 μM: $N = 4$, $n = 5$, $P = 0.10$; 2 μM: $N = 4$, $n = 5$, $P = 0.13$; 4 μM: $N = 4$, $n = 6$, $P = 0.03$; 8 μM: $N = 6$, $n = 9$, $P = 0.004$, Wilcoxon test; WT vs. *Df(16)A*$^{+/-}$: $P = 0.69$, two-way ANOVA). (*C*) Dose-dependent decrease in first spike latency in WT mice (before and after NMDA, 0 μM: $n = 4$, $P = 0.13$; 1 μM: $n = 4$, $P = 0.13$; 2 μM: $n = 5$, $P = 0.13$; 4 μM: $n = 5$, $P = 0.06$; 8 μM: $n = 7$, $P = 0.02$, Wilcoxon test) is not statistically different from *Df(16)A*$^{+/-}$ mice (0 μM: $n = 4$, $P = 0.75$, 1 μM: $n = 5$, $P = 0.63$, 2 μM: $n = 5$, $P = 0.06$, 4 μM: $n = 6$, $P = 0.03$; 8 μM: $n = 9$, $P = 0.004$, Wilcoxon test; WT versus *Df(16)A*$^{+/-}$: $P = 0.25$, two-way ANOVA). (*D* and *E*) Quinpirole (0.8 μM) blocked pyramidal neuron excitability induced by NMDA in WT (28.4 ± 16.0% increase from baseline, $N = 4$, $n = 8$, $P = 0.29$, Wilcoxon test) but not in *Df(16)A*$^{+/-}$ mice (106.2 ± 24.7% increase, $N = 4$, $n = 7$, $P = 0.02$, Wilcoxon test). (*F*) Summary of the inhibitory effect of quinpirole on the NMDA-induced neuronal excitability. 4 μM NMDA increased the number of spikes by 103.9 ± 26.6% in WT and 115.8 ± 25.8% in *Df(16)A*$^{+/-}$ mice, respectively. However, 0.8 μM quinpirole significantly blocked cell excitability in WT (NMDA only vs. NMDA+Quinpirole: $P = 0.02$, Mann–Whitney test) but not in *Df(16)A*$^{+/-}$ mice (NMDA only vs. NMDA+Quinpirole: $P = 0.51$ Mann–Whitney test). Bottom traces represent the inhibitory effect of quinpirole on NMDA-induced excitability of WT and *Df(16)A*$^{+/-}$ mice. Data are shown as mean ± SEM. $^{*}P < 0.05$, $^{\#}P < 0.05$, $^{\#\#}P < 0.01$.

significantly reduced the excitatory effect of 4 μM NMDA in WT (Fig. 3*D–F*). However, the D2 attenuation of the excitatory effect of NMDA was not observed in the *Df(16)A*$^{+/-}$ mice (Fig. 3*D–F*). Overall, our data suggest that the specific inhibitory action of D2Rs on pyramidal neuron excitatory transmission is compromised in the PFC of *Df(16)A*$^{+/-}$ mice.

D2R-Mediated Attenuation of PFC Pyramidal Neuron Excitability Involves GABAergic Transmission

Inhibitory neuron dysfunction is one of the diverse features affecting neural circuits underlying susceptibility to SCZ (Marin 2012). Therefore, we wondered whether altered GABAergic transmission and/or its modulation are involved in the abnormal D2 attenuation of PFC pyramidal neuron excitability. Bath application of 10 μM bicuculline almost completely attenuated the quinpirole-induced-inhibitory effect in WT but not in *Df(16)A*$^{+/-}$ mice (Fig. 4A,B). This finding suggests that the attenuation of pyramidal neuron excitability is mediated by increased GABA release from GABA interneurons by quinpirole. Consistent with this finding, application of 2 μM quinpirole significantly increased the frequency of sIPSC in WT mice while had no effect on *Df(16)A*$^{+/-}$ mice (Fig. 4C). By comparison, the excitatory effect of D1R on pyramidal neurons was not blocked by bicuculline (see Supplementary Fig. S4) indicating that D1R predominately affects pyramidal neurons.

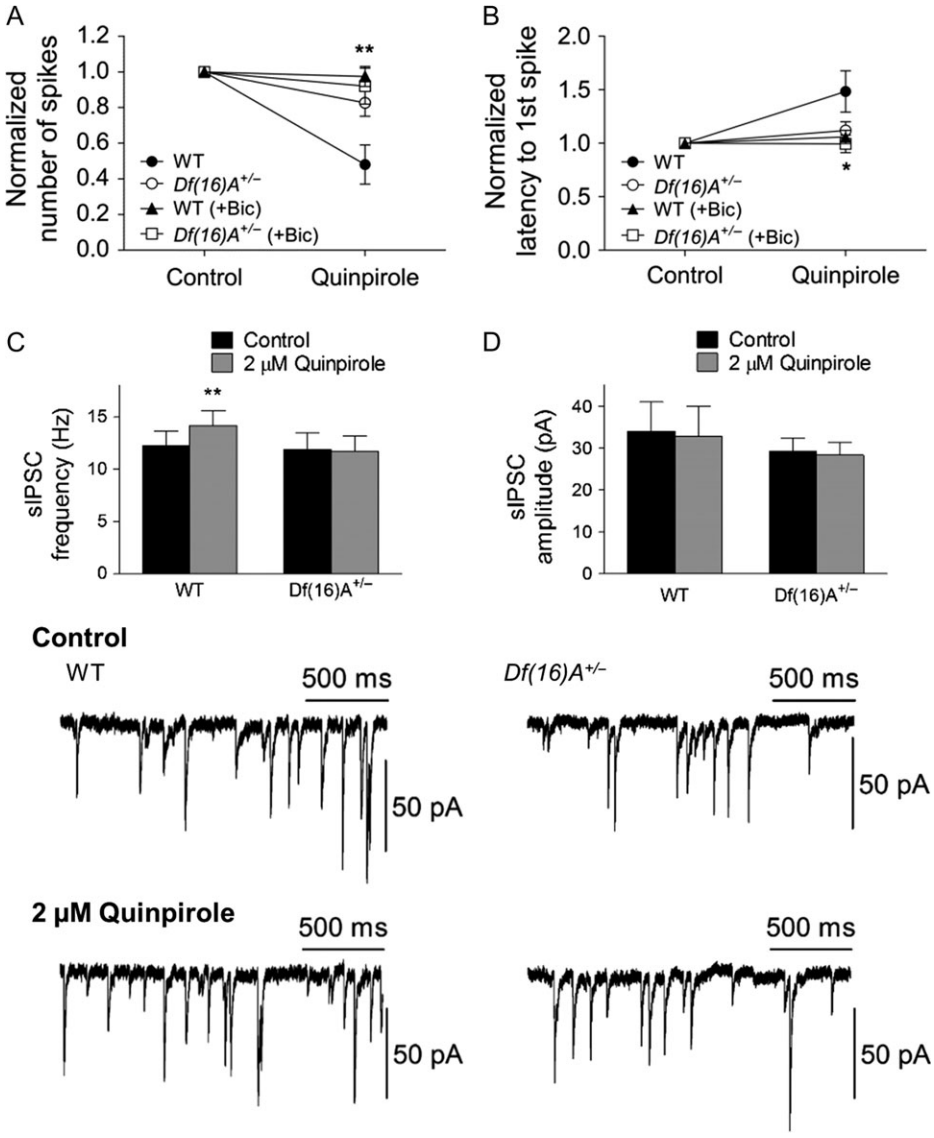

Figure 4. Involvement of GABAergic transmission in the D2R modulation of PFC pyramidal neuron excitability. (*A*) Bath application of 10 μM bicuculline attenuated the quinpirole-induced-inhibitory effect on the number of spikes in WT (before and after quinpirole; 14.7 ± 8.7% decrease from baseline, $N = 6$, $n = 10$, $P = 0.44$, Wilcoxon test; quinpirole only vs. quinpirole+bicuculline: $P = 0.002$, Mann–Whitney test) but not in *Df(16)A*$^{+/-}$ mice (before and after quinpirole: 7.9 ± 10.1% decrease from baseline, $N = 7$, $n = 10$, $P = 0.24$, Wilcoxon test; quinpirole only vs. quinpirole+bicuculline: $P = 0.90$, Mann–Whitney test). The asterisk indicates the significance between quinpirole only and quinpirole+bicuculline in WT mice. (*B*) Bicuculline attenuated the effect of quinpirole on the latency to first spike in WT (before and after quinpirole: 11.9 ± 0.1% from baseline, $n = 10$, $P = 0.36$, Wilcoxon test; quinpirole only vs. quinpirole+bicuculline: $P = 0.04$, Mann–Whitney test) and *Df(16)A*$^{+/-}$ mice (before and after quinpirole: 0.5 ± 8.1% from baseline, $n = 10$, $P = 0.67$, Wilcoxon test; quinpirole only vs. quinpirole+bicuculline: $P = 0.40$, Mann–Whitney test). (*C*) The frequency of sIPSC was significantly increased by quinpirole in WT (control, 12.3 ± 1.4 Hz; quinpirole, 14.2 ± 1.4, $n = 14$, $P = 0.004$, Wilcoxon test) but not in *Df(16)A*$^{+/-}$ mice (control, 11.9 ± 1.6 Hz; quinpiriole, 11.7 ± 1.5, $n = 13$, $P = 0.68$, Wilcoxon test). (*D*) No significant change by quinpirole on the amplitude of sIPSC both in WT (control, 34.0 ± 7.0 pA; quinpirole, 32.9 ± 7.0 pA, $n = 14$, $P = 0.45$, Wilcoxon test) and *Df(16)A*$^{+/-}$ mice (control, 29.3 ± 3.2 pA; quinpiriole, 28.4 ± 3.0 pA, $n = 13$, $P = 0.60$). Bottom panel illustrates representative traces of before and after quinpirole treatment on the sIPSC recorded from single pyramidal neurons in WT and *Df(16)A*$^{+/-}$ mice. Data are shown as mean ± SEM. *$P < 0.05$, **$P < 0.01$.

D2R-Mediated Enhancement of PFC PV+ Interneuron Excitability is Reduced in *Df(16)A*$^{+/-}$ Mice

To directly investigate whether enhancement of PV+ interneuron firing by activation of D2R is decreased in *Df(16)A*$^{+/-}$, we performed current-clamp in layer V PV+ interneurons. To achieve cellular specificity, *Df(16)A*$^{+/-}$ mice were crossed with GAD67-GFP mice (Chattopadhyaya et al. 2004) to generate *Df(16)A*$^{+/-}$; GAD67-GFP$^{+/-}$ and WT littermates in which PV+ interneurons are labeled by GFP. GFP neurons exhibited pronounced afterhyperpolarization (AHP, 19.0 ± 3.5 mV), short action potential duration (0.52 ± 0.07 ms at half amplitude), and lack of spike-frequency adaptation (the ratio between the last and first interspike interval <1.3), low input resistance (<200 MΩ), all characteristics of fast-spiking PV+ interneurons (Rudy et al. 2010) (Fig. 5A). We first examined the passive membrane and firing properties of the PV+ interneurons, and did not find any alteration of the IV relationship (Fig. 5B), and no difference in resting membrane potential (WT: −73.6 ± 0.6 mV, $N = 26$, $n = 51$; *Df(16)A*$^{+/-}$: −75.0 ± 0.9 mV, $N = 18$, $n = 34$, $P = 0.24$) and input resistance (WT: 131.5 ± 8.0 MΩ, $N = 26$, $n = 51$; *Df(16)A*$^{+/-}$: 132.0 ± 7.1 MΩ, $N = 18$, $n = 34$, $P = 0.97$). There was no difference between WT and *Df(16)*$^{A+/-}$ neurons in the spike frequency in a range of depolarizing currents (Fig. 5C). Thus, the 22q11.2 microdeletion does not appear to alter the excitability of layer V PV+ neurons at baseline.

We next determined the effect of quinpirole on PV+ interneuron excitability. Bath application of 2 μM quinpirole induced greater increase in PV+ interneuron excitability in the WT mice (1.6 ± 0.5-fold increase) while having little effect on *Df(16)A*$^{+/-}$ mice (0.2 ± 0.1-fold increase) (Fig. 5D–F). The effect is D2R dependent since sulpiride completely blocked the effect (Fig. 5D). This finding strongly indicates the weaker D2R-induced attenuation of pyramidal neuron firing in the *Df(16)A*$^{+/-}$ mice is mainly due to the weaker increase in interneuron firing (and presumably GABA release) by D2R activation. Thus, dopaminergic modulation of the coordination between pyramidal and GABAergic interneuron activity is altered in *Df(16)A*$^{+/-}$ mice leading to an increased excitation upon dopaminergic challenge.

Midbrain DA neurons are intrinsic pacemakers. Thus endogenous dopaminergic tone is always present in vivo and may even be elevated in the PFC of *Df(16)A*$^{+/-}$ mice due to lower COMT activity and reduced clearance of DA (Kaenmaki et al. 2010). This could lead to a ceiling effect of quinpirole action in *Df(16)A*$^{+/-}$ mice in vivo. However, the coronal PFC slices should have little endogenous DA release since there are no DA neurons present in the preparation and, therefore, the reduced D2R response in PFC slices from *Df(16)A*$^{+/-}$ mice observed in our study is unlikely due to the ceiling effect. Nevertheless, to confirm that the tonic endogenous DA level in the PFC slices is low, we examined the effect of D2 antagonist alone on pyramidal neurons and PV+ interneurons. Sulpiride alone had no effect on the excitability of pyramidal neurons (see Supplementary Fig. S5A) and PV+ interneurons (see Supplementary Fig. S5B) in both WT and *Df(16)A*$^{+/-}$ mice thus excluding the contribution of a DA ceiling effect. This finding is consistent with the observation that DA levels in the PFC of WT and *Df(16)A*$^{+/-}$ mice are not significantly different (measured by HPLC, WT: 139.6 ± 21.2 ng/g tissue, $N = 7$; *Df(16)A*$^{+/-}$: 107.9 ± 9.6 ng/g tissue, $N = 7$, $P = 0.21$, *t*-test) , which suggests

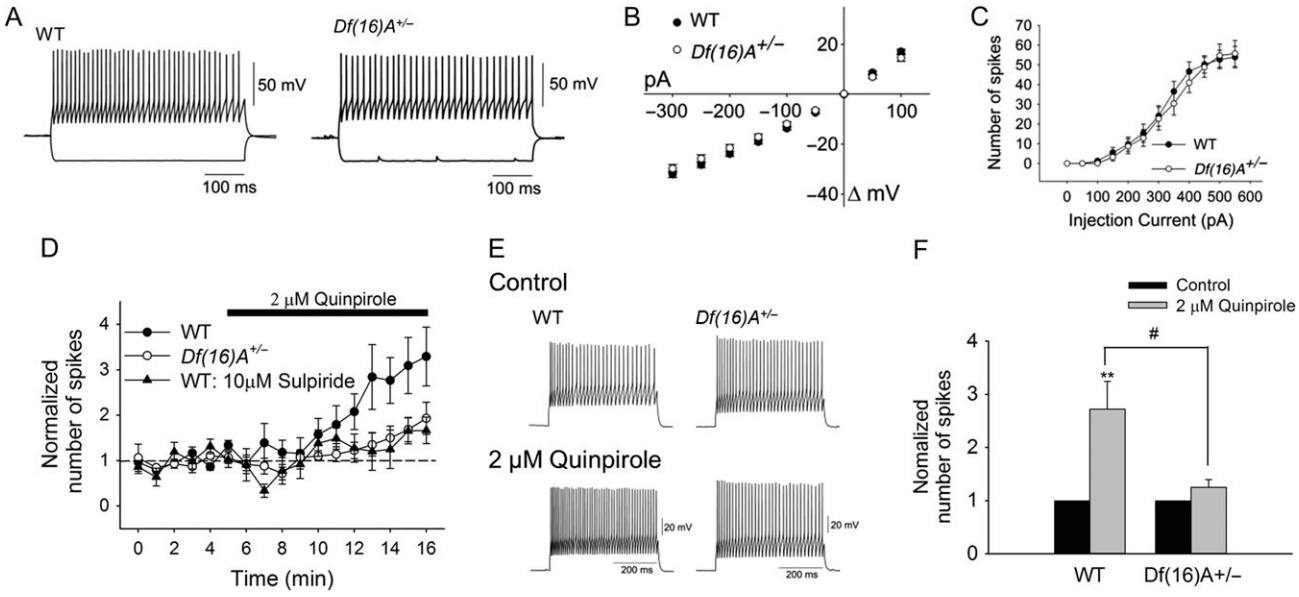

Figure 5. The excitatory effect of quinpirole on PFC PV+ interneuron excitability is reduced in *Df(16)A*$^{+/-}$ mice. (*A–C*) Whole-cell recordings of PFC layer V PV+ GABAergic interneurons from WT and *Df(16)A*$^{+/-}$ mice show normal excitability. (*A*) Representative traces of voltage responses to depolarizing and hyperpolarizing somatic step current injection (−300 to +450 pA) from WT (top left) and *Df(16)A*$^{+/-}$ (top right) mice. No difference in resting membrane potential and input resistance was detected. (*B*) IV plot obtained from the traces shown in (*A*) for WT ($N = 17$, $n = 45$) and *Df(16)A*$^{+/-}$ ($N = 7$, $n = 14$), WT versus *Df(16)A*$^{+/-}$: $P = 0.11$, two-way ANOVA. (*C*) No difference in the excitability of PV+ interneurons was observed between WT ($N = 9$, $n = 21$) and *Df(16)A*$^{+/-}$ mice ($N = 8$, $n = 15$), WT versus *Df(16)A*$^{+/-}$: $P = 0.39$, two-way ANOVA. (*D*) Bath application of 2 μM quinpirole induced greater increase in the cell excitability in WT (before and after quinpirole: 161.9 ± 52.6% increase from baseline, $N = 9$, $n = 15$, $P = 0.0004$, Wilcoxon test) than *Df(16)A*$^{+/-}$ mice (before and after quinpirole: 24.8 ± 14.6% increase from baseline, $N = 4$, $n = 8$, $P = 0.08$, Wilcoxon test). Triangle indicates that pretreatment with 10 μM sulpiride blocks the excitatory effect of quinpirole on WT mice (before and after quinpirole: 17.0 ± 16.5% increase from baseline, $n = 4$, $P = 0.38$, Wilcoxon test; quinpirole only versus quinpirole+sulpiride: $P = 0.02$, Mann–Whitney test). (*E*) Representative traces illustrate the quinpirole effect on the action potential firing induced by depolarizing current injection (250–450 pA) in single neurons from WT and *Df(16)A*$^{+/-}$ mice. (*F*) The bar graph depicts the significant increase in cell firing by quinpirole in WT but not in *Df(16)A*$^{+/-}$ mice (WT: 1.6 ± 0.5-fold increase, $n = 15$; *Df(16)A*$^{+/-}$: 0.2 ± 0.1-fold increase, $n = 8$, $P = 0.012$, Mann–Whitney test). Data are shown as mean ± SEM. $^{\#}P < 0.05$, $^{***}P < 0.001$.

that the DA content in the DA terminals present in PFC slices is not altered in the *Df(16)A*$^{+/-}$ mice.

Impaired D2R Modulation of PV+ Interneuron Excitability in *Df(16)A*$^{+/-}$ Mice is Mediated by Reduced Kv7/KCNQ/M-type Potassium Channel Activity

The lack of the D2R ability to activate PV+ interneurons could in principle arise from reduced D2R expression, altered downstream signaling pathways and substrates, or both. To test the first possibility, we performed quantitative reverse transcription-PCR (qRT-PCR) in the PFC of *Df(16)A*$^{+/-}$ mice and WT littermates. The D2R gene (*Drd2*) abundance was slightly elevated in the *Df(16)A*$^{+/-}$ mice compared with WT mice (see Supplementary Fig. S6A). We also performed immunohistochemistry for D2Rs in the PFC of *Df(16)A*$^{+/-}$ mice and WT littermates. Quantification of D2R levels in PV+ cells did not show reduction in the protein levels but consistent with the qRT-PCR results revealed a slight increase in protein levels in *Df(16)A*$^{+/-}$ mice compared with their WT littermate (see Supplementary Fig. S6B-S6C). Thus, reduction in D2R levels is not the underlying molecular mechanism for the D2R inability to activate PV+ interneurons. The observed slight elevation in RNA and protein levels likely reflects a compensatory change.

There are a number of other possibilities that could explain the loss of D2 modulation of PV+ interneuron excitability in *Df(16)A*$^{+/-}$ mice. Potassium conductance is known to regulate neuronal excitability. We, therefore, reasoned that the Kv7/KCNQ/M-type K channel was a good candidate, as the M-current is widely present in CNS, activates at subthreshold voltages, and is a releasable restraint on neuronal excitability (Delmas and Brown 2005; Lawrence et al. 2006; Cooper 2011). Most importantly it is functionally coupled to D2Rs (Ljungstrom et al. 2003). We first investigated whether KCNQ channels are involved in the D2R modulation of PV+ interneuron excitability by pretreating slices with KCNQ-channel blocker, XE991. Notably, XE991 at a concentration of 4 μM significantly attenuated the excitatory effect of quinpirole on PV+ interneurons in WT (from 2.6 ± 0.5 to 1.3 ± 0.2), while having no effect on *Df(16)A*$^{+/-}$ mice as expected (Fig. 6A,B). This data suggests that KCNQ channels are involved in the D2 modulation of PV+ interneuron excitability. Application of 4 μM XE991 increased PV+ interneuron excitability significantly more in WT compared with *Df(16)A*$^{+/-}$ (2.4-fold versus 0.8-fold), indicating a decrease in the activity of KCNQ channels in the PV+ interneuron of *Df(16)A*$^{+/-}$ (see Supplementary Figs S7A and S7B). To directly determine the activity of KCNQ channels in PV+ neurons, KCNQ currents were examined using a standard deactivation protocol (Brown and Adams 1980). Neurons were held at −20 mV to minimize contamination from currents such as A-type potassium current. KCNQ-like currents were visualized with a 0.5-s-long hyperpolarizing voltage steps from −20 mV to −30 ~ −40 mV. XE991-sensitive-KCNQ-channel currents were obtained by digital subtraction of the traces before and after 10 μM XE991 application (see Supplementary Fig. S8A, S8B). Consistent with the current-clamp results (see Supplementary Fig. S7A, S7B), WT mice showed greater average current amplitude than *Df(16)A*$^{+/-}$ mice either by perforated or by whole-cell patch-clamp recording (Fig. 6C and see Supplementary Fig. S9). To test whether activation of D2Rs in PV interneurons leads to KCNQ closure and thereby increase in firing, we measured the XE991-sensitive-KCNQ current in the presence of quinpirole and found it to be suppressed. Consistently, quinpirole sensitive current was suppressed in the presence of XE991 (Fig. 6E,F). Furthermore, XE991 treatment blocked the quinpirole-induced increase in sIPSCs in pyramidal neurons, confirming that reduced KCNQ function in the PV+ interneurons of *Df(16)A*$^{+/-}$ mice renders them less capable of inhibiting pyramidal cells upon D2R modulation (see Supplementary Fig. S10). Among the five Kv7/KCNQ-channel subtype, KCNQ2/3 seem to have a prominent role in most neurons (Wang et al. 1998) and KCNQ2 is expressed in PV+ interneurons (Nieto-Gonzalez and Jensen 2013). In agreement with these findings, we observed that KCNQ2 is expressed in PV+ interneurons in the PFC (Fig. 6D). Moreover, compared With PV+ interneurons, we found much weaker expression of KCNQ2 in non-PV+ cells (~40% of expression in PV+ cells based on the fluorescent intensity), an observation consistent with the little M-current observed in layer V pyramidal neurons (see Supplementary Fig. S11A, S11B). It should be noted that KCNQ located on dendrites and spines would not be detected using our technique. Consistent with previous findings in mice and rats indicating that KCNQ channels are expressed at higher levels in layer II/III pyramidal neurons (Santini and Porter 2010; Arnsten et al. 2012) we detected more robust XE991-sensitive (KCNQ) current (~53 pA) in layer II/III pyramidal neurons (see Supplementary Fig. S12A, S12B), a finding that may be related to the opposite effects of quinpirole application on pyramidal neurons in these two layers. Consistently, XE991 increased layer II/III pyramidal neurons activity more effectively than layer V (see Supplementary Fig. S12C). Regional and neuronal-type dependent differences in the expression of KCNQ channels in the mouse brain notwithstanding, our findings strongly suggest that KCNQ2 is a plausible candidate to mediate the loss of D2R modulation of PV+ interneuron excitability in layer V of the PFC of *Df(16)A*$^{+/-}$ mice.

Double immunohistochemistry combined with quantification of KCNQ2 levels in PV+ cells revealed a significant 20% decrease of KCNQ2 levels in PV+ cells in *Df(16)A*$^{+/-}$ mice compared with their WT littermates (Fig. 6D). We did not detect any genotypic difference in either KCNQ2 levels or KCNQ-channel activity in layer V pyramidal neurons (see Supplementary Fig. S10). Thus, reduction of KCNQ2 levels may be contributing in part to the observed decrease in M-current in layer V PV+ interneurons.

The molecular interactions of DRD2 and KCNQ2-dependent interneuron excitability may transcend the 22q11.2 deletion and have more general implications for understanding the genetic risk for mental illnesses. We assess the statistical evidence for an epistatic genetic interaction between *KCNQ2* and *DRD2* genes in association with SCZ risk, that is the possibility that genetic variants that affect the function, expression or splicing of the 2 genes have different effects on disease-risk in combination than individually, by analyzing the PGC SCZ case/control data set (Consortium 2011) (see Supplementary Table 1).

Given that these two genes reside on different chromosomes we expect all variants in these genes to be in linkage equilibrium, which is independently and randomly inherited in healthy control individuals. However, if there is an interaction between *KCNQ2* and *DRD2* genes in association with SCZ risk, at least some variants, specifically ones that have an impact on the function, expression or splicing of the genes, should be in linkage disequilibrium, that is nonrandomly co-inherited at frequencies significantly different than expected by chance, only in SCZ cases. We tested this hypothesis by extracting genotypes of all SNPs within the *KCNQ2* and *DRD2* genomic regions from the 8024 SCZ cases and 7798 controls of the PGC SCZ data set and conducting a pair-wise interaction comparison between the SCZ and control groups as implemented in pLINK (http://pngu.mgh.harvard.edu/~purcell/plink), a well-established statistical software to detect such interaction. We used the permutation option within the pLINK software to control for multiple-testing.

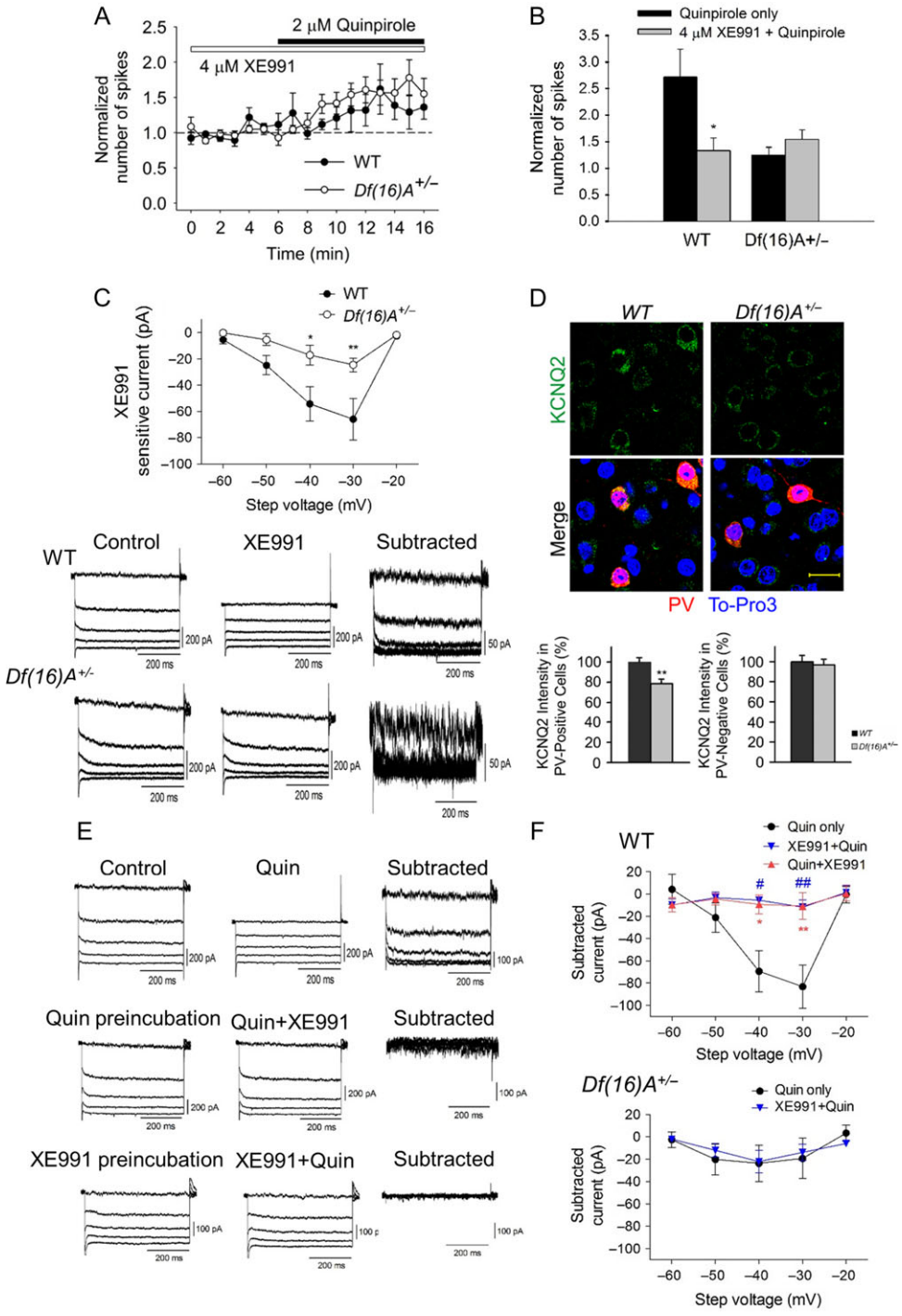

Figure 6. Involvement of KCNQ potassium channels in the D2R modulation of PFC PV+ interneuron excitability. (*A*) Time-course plotted graph showing that pretreatment with KCNQ-channel blocker, XE991 attenuated the excitatory effect of quinpirole on PV+ interneurons in WT but not in *Df(16)A*$^{+/-}$ mice. (*B*) XE991 significantly reduced the increase in the number of spikes by quinpirole in WT (quinpirole only: 1.6 ± 0.5-fold increase, $n = 15$; quinpirole + XE991: 0.3 ± 0.2-fold increase, $n = 9$, $P = 0.02$, Mann–Whitney test) but not in *Df(16)A*$^{+/-}$ mice (quinpirole only: 0.2 ± 0.1-fold increase, $n = 8$; quinpirole + XE991:0.5 ± 0.2-fold increase, $n = 7$, $P = 0.39$, Mann–Whitney test). (*C*) Whole-cell voltage recording of XE991-sensitive-KCNQ-channel currents. WT mice ($N = 9$, $n = 13$) showed greater average current amplitude than *Df(16)A*$^{+/-}$ mice ($N = 7$, $n = 10$, WT versus *Df(16)A*$^{+/-}$: $P = 0.0002$, two-way ANOVA; WT vs. *Df(16)A*$^{+/-}$: −40 mV: $P < 0.05$, −30 mV: $P < 0.01$). Representative traces on the bottom illustrate bigger XE991-sensitive currents in WT than in *Df(16)A*$^{+/-}$ mice. KCNQ currents were digitally subtracted from currents evoked by voltage steps (−60 to −20 mV) from −20 mV before and after 10 μM XE991 treatment in the presence of 1 μM TTX. (*D*) KCNQ channels expression was reduced in the PFC PV+ interneuron of *Df(16)A*$^{+/-}$ mice. Top panel shows representative images from immunohistochemical analysis of expression of KCNQ2 (*green*) in PV+ cells (*red*) in PFC from WT and *Df(16)A*$^{+/-}$ mice. Nuclei were stained with TO-PRO 3 (*blue*). *Scale bar*: 20 μm. Bottom panel shows the quantification of KCNQ2 in PV-positive cells and PV-negative cells ($N = 6$, $n = 54$ each genotype). (*E*) Representative traces from WT mice illustrate that quipirole inhibited KCNQ currents and XE991 attenuated the effect of quinpirole on KCNQ currents. (*F*) Quinpirole inhibited XE991-sensitive-KCNQ currents. Quinpirole inhibited the potassium currents at a similar level to XE991-sensitive-KCNQ currents as shown in (*C*) (filled-circle, WT: quinpirole, $n = 13$; XE991, $n = 12$, $P = 0.67$; *Df(16)A*$^{+/-}$: quinpirole, $n = 10$; XE991, $n = 10$, $P = 0.66$, two-way ANOVA). Quinpirole preincubation attenuated the effect of XE991 on the potassium currents (XE991, $n = 13$; quinpirole+XE991, $n = 6$, $P = 0.005$, two-way ANOVA). Preincubation of XE991 attenuated the inhibitory effect of quinpirole on the potassium currents (blue reverse triangle, quinpirole, $n = 13$; XE991+quinpirole, $n = 8$, $P = 0.01$, two-way ANOVA). Bottom panel shows preincubation of XE991 had no effect of quinpirole on the potassium currents in *Df(16)A*$^{+/-}$ mice (quinpirole only, $n = 10$; XE991+quinpirole, $n = 10$, $P = 0.85$, two-way ANOVA). Data are shown as mean ± SEM $^{*}P < 0.05$, $^{\#}P < 0.05$, $^{**}P < 0.01$, $^{\#\#}P < 0.01$.

A significant interaction difference (that is a differential occurrence of certain combinations of genotypes) was found between SCZ cases and controls for the SNP pair rs4936270 in *DRD2* and rs6089908 in *KCNQ2* (odd ratio = 1.88, *P*-value of 0.0011; *P*-value = 0.02 following permutations). Both are intronic SNPs (see Supplementary Table 1) and, importantly, none of them showed main association with SCZ risk on their own. Whether these SNPs themselves affect aspects of expression or splicing of either gene or are merely linked to juxtaposed culprit SNPs remains to be determined. Nevertheless, these results suggest that *DRD2* and *KCNQ2* family of channels may interact to affect SCZ risk in general and not only at the 22q11.2 locus.

D2R Modulates of KCNQ-Dependent Interneuron Excitability via GSK-3β

KCNQ2 channel activity is dependent on its state of phosphorylation (Hoshi et al. 2003) and could be modulated by several different signaling pathways (Delmas and Brown 2005). GSK-3β phosphorylates KCNQ2 channel leading to its closure (Borsotto et al. 2007; Kapfhamer et al. 2010). The well-established link between D2R and GSK-3β activity (Beaulieu et al. 2009) prompted us to examine whether GSK-3β mediates the effect of D2 activity on KCNQ channels. Pretreatment of cortical slices with GSK-3β inhibitor, TDZD blocked the excitatory effect of quinpirole on PV+ interneurons (Fig. 7A, B) and attenuated the excitatory effect of XE991 on PV+ interneurons in WT mice (Fig. 7C). Consistently, TDZD blocked the quinpirole sensitive-KCNQ current (Fig. 7D). These findings suggest that D2 modulation of KCNQ-dependent interneuron excitability is mediated via GSK-3β pathway, that is, activation of D2Rs leads to activation of GSK-3β, and then results in the closure of KCNQ channels. As expected by the reduction of KCNQ2 channel currents, no evidence for significant modulation of PV+ interneuron excitability by TDZD pretreatment was observed in similar analysis of *Df(16)A*$^{+/-}$ mice (Fig. 7C).

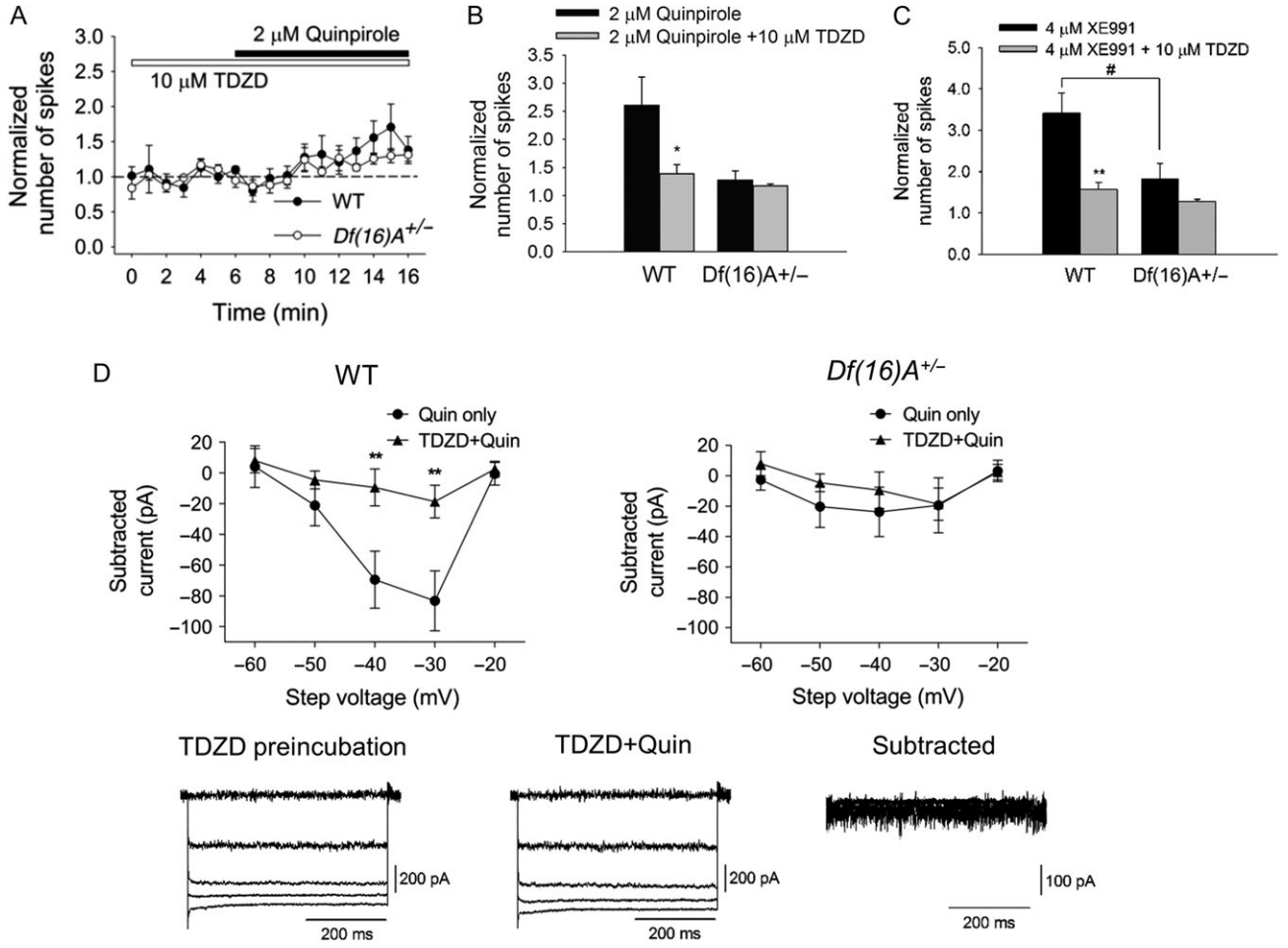

Figure 7. GSK-3β mediates D2R modulation of PV+ interneuron excitability in the PFC, through KCNQ channels. (*A*) Time-course plotting showing that pretreatment with GSK-3β inhibitor, TDZD attenuated the excitatory effect of quinpirole on PV+ interneurons in WT ($N = 5$, $n = 9$) but not in *Df(16)A*$^{+/-}$ mice ($N = 6$, $n = 8$). (*B*) TDZD significantly reduced the increase in the number of spikes by quinpirole in WT (quinpirole only: 1.6 ± 0.5-fold increase, $n = 15$; quinpirole + TDZD: 0.4 ± 0.2-fold increase, $n = 9$, $P < 0.05$, Mann–Whitney test) but not in *Df(16)A*$^{+/-}$ mice (quinpirole only: 0.2 ± 0.1-fold increase, $n = 8$; quinpirole + TDZD: 0.17 ± 0.04-fold increase, $n = 8$, $P = 0.96$, Mann–Whitney test). (*C*) TDZD significantly reduced the increase in the number of spikes by XE991 in WT (XE991 only: 2.4 ± 0.5-fold increase, $n = 8$; XE991+TDZD: 0.6 ± 0.2-fold increase, $n = 7$, $P < 0.01$, Mann–Whitney test) but not in *Df(16)A*$^{+/-}$ mice (XE991 only: 0.8 ± 0.4-fold increase, $n = 7$; XE991+TDZD: 0.27 ± 0.07-fold increase, $n = 5$, $P = 0.27$, Mann–Whitney test). WT versus *Df(16)A*$^{+/-}$, XE991 only: $P < 0.05$; XE991+TDZD: $P = 0.52$, Mann–Whitney test. (*D*) Preincubation of TDZD attenuated quinpirole effect on KCNQ currents in WT (quinpirole only, $n = 10$; TDZD + quinpirole, $n = 10$, $P < 0.01$, two-way ANOVA) but not in *Df(16)A*$^{+/-}$ mice (quinpirole only, $n = 7$; TDZD + quinpirole, $n = 7$, $P = 0.65$, two-way ANOVA). Bottom panel: representative traces illustrate that TDZD attenuated the effect of quinpirole. Data are shown as mean ± SEM. *$P < 0.05$; **$P < 0.01$.

Discussion

The integration of excitatory and inhibitory inputs at the level of the individual neuron, and neural circuits, modulates circuit activation threshold and responsiveness and is fundamental to the brain information processing. A growing body of evidence suggests that disruption of excitatory and inhibitory set points may be implicated in a range of neurodevelopmental disorders (Yizhar et al. 2011; Marin 2012). In most of these cases (almost exclusively autism models), pathogenic mutations lead to pronounced imbalances, beyond the control of homeostatic responses, primarily due to altered formation, maintenance or selective loss of either excitatory or inhibitory neurons or synapses. Previous evaluation of inhibitory neuronal density in a mouse model of the 22q11.2 deletion revealed a subtle decrease in PV+ prefrontal cortical inhibitory neurons in layer V (Fenelon et al. 2013) but whether this change is accompanied by alterations in the functional properties of inhibitory neurons remained unknown. Here, we show that the same mouse model shows normal excitability of pyramidal neurons and interneurons and normal ratio of excitatory versus inhibitory synaptic transmission at baseline, strongly arguing against attributing the primary circuit deficits in this mouse model to a straightforward wholesale reduction of GABAergic action. By contrast, these properties are altered under dopaminergic modulation at least in part due to a finer-scale abnormal functionality of cortical interneurons.

To the best of our knowledge, this is the first study to address how the pattern of excitatory/inhibitory balance is altered by a genuine SCZ-predisposing mutation. We reveal a pattern where the relative contribution of excitatory and inhibitory neurons is altered only upon neuromodulation. DA neuromodulation of PFC circuits has been extensively studied, but the majority of these studies have been conducted in juvenile rats and mice (Gao and Goldman-Rakic 2003; Durstewitz and Seamans 2008; Tseng et al. 2008; Ji et al. 2009) when DA signaling in PFC has not matured (Paul and Cox 2013). Indeed, this is the first study to address how DA neuromodulation is altered in the mature cortex of a mouse model of a genuine SCZ-predisposing mutation.

Coronal PFC slices contain little extracellular DA and therefore the normal balance of excitatory versus inhibitory synaptic transmission observed in our recordings likely reflects default intrinsic properties of the mutant network. On the other hand, PFC receives dopaminergic input from the ventral tegmental area and cortical DA is known to play an important role in PFC-dependent cognitive functions, such as WM, reward-seeking, and attention (Brozoski et al. 1979; Williams and Goldman-Rakic 1995; Schultz 2002; Gao and Goldman-Rakic 2003; O'Donnell 2003; Vijayraghavan et al. 2007; Durstewitz and Seamans 2008; Gruber et al. 2010; Arnsten et al. 2012). Thus, endogenous dopaminergic tone is always present in vivo and may even be elevated in the PFC of *Df(16)A*$^{+/-}$ mice due to lower COMT activity and reduced clearance of extracellular DA (Kaenmaki et al. 2010). Therefore, local PFC circuits in *Df(16)A*$^{+/-}$ mice that normally depend on DA activity may not be able to integrate properly excitatory and inhibitory influences due to a combination of altered responsiveness to DA receptor activation (reduced inhibitory effect on excitability upon D2R activation and enhanced excitability upon D1R activation) and increased dopaminergic tone (reduced COMT activity).

In that context, our data support a model in which the 22q11.2 deletion results in altered DA neuromodulation of PV+ interneurons and an aberrant DA-depended coordination between pyramidal and GABAergic interneurons. This has several potentially important implications. The lack of activation of interneurons would contribute to reduced attenuation of irrelevant inputs (O'Donnell 2003) and noisy information processing in the PFC and may result, for example, in poor assignment of saliency to sensory information associated with a surge in DA when DA neurons fire in response to unexpected reward or reward-predicting stimuli (Schultz 2002) or in impaired DA-modulated prefrontal cognitive operations such as attention, WM, and other executive functions (Goldman-Rakic et al. 2000; O'Donnell 2003; Arguello and Gogos 2010). Moreover, under condition such as mild stress when there is increased DA release in PFC (Nagano-Saito et al. 2013) or when 22q11.2 deletion carriers co-inherit mutations that elevate dopaminergic tone (Paterlini et al. 2005), E/I imbalance could be elevated further resulting in impaired PFC cognitive and behavioral operations. Finally, it is conceivable that abnormal dopaminergic modulation may contribute to a wider range of disease symptoms depending on the cortical region primarily affected by the alteration of interneurons. Therefore, our results may offer more general insights into the nature of the neural substrates underlying 22q11.2-associated cognitive and psychiatric phenotypes. The effects of the highly heterogeneous collection of pathogenic mutations predisposing to SCZ likely converge on the level of neural circuits and specifically on how they affect the temporal and, possibly, spatial dynamics of intricately connected neuronal populations (Arguello and Gogos 2011; Crabtree and Gogos 2014), providing plausible links to specific symptoms that differentiate, for example, SCZ from other neuropsychiatric and neurodevelopmental syndromes. Along these lines, we have previously described alterations in the long and short-range connectivity, stability, and plastic properties of neuronal circuits in the 22q11.2 mouse model (Drew et al. 2011; Fenelon et al. 2011, 2013; Ellegood et al. 2014; Xu et al. 2013; Tamura et al. 2016). Indeed, it has been well established that both the rhythmic activity and synaptic plasticity in the cortex is dependent upon properly balanced excitatory and inhibitory influences (Haider et al. 2006; Zhang et al. 2011), which are to a large extent under neuromodulation, including modulation by DA. In that context, here, we provide intriguing evidence suggesting that abnormal dopaminergic modulation of excitatory/inhibitory influences may impose additional burden on the dynamics of neural networks in 22q11.2 deletion carriers. Relevant to this line of reasoning, is also the realization that the genetic contribution of large copy number variants, such as the 22q11.2 deletions involve additive or synergistic interaction of multiple genes within the region, that is a degree of "micro-complexity" that reflects and provides insights to the more extensive genetic "macro-complexity" inherent in the genetic architecture of mental disorders (Sanders et al. 2015).

Our model captures the essence of a DA-dependent imbalance in excitatory and inhibitory influences in the PFC of *Df(16)A*$^{+/-}$ mice, but it is most likely incomplete.

First, in addition to D2, D3 and D4 receptors are also highly expressed in PFC. Activation of D4Rs have been shown to decrease sIPSC in the PFC layer V pyramidal neurons (Zhong and Yan 2014), in a manner opposite to the effect of quinpirole on sIPSC in the pyramidal neurons. D3Rs are unique among the D2-like receptors in exhibiting sustained high affinity for DA (>20-fold higher than D2Rs), suggesting that endogenous DA may occupy D3Rs in vivo for extended periods of time, leading to high spontaneous activation of these receptors and a possible attenuation of any effects of DA level fluctuations during phasic DA release (Richtand et al. 2001). Along these lines, it

should be also noted that the impaired D2R function in the mutant mice revealed by quinpirole (which stimulates both D2Rs and D3Rs) could be due to additional alterations in D3R signaling. Future studies using specific D3R antagonists could distinguish the contribution of each type of receptor.

Second, we have also found that the excitatory action of D1R was enhanced in *Df(16)A*$^{+/-}$ mice, which will also contribute to altered E/I balance in *Df(16)A*$^{+/-}$ mice during dopaminergic modulation. Whereas this excitatory effect is restricted mainly on pyramidal neurons, consistent with many other studies (Tseng and O'Donnell 2004; Chen et al. 2007), further experimentation will be required to determine the molecular mechanisms underlying this enhanced excitability. These may include alterations in PKA- or PKC-dependent pathways and in the levels of Ca^{2+}, K^+, and Na^+ channels (Dong and White 2003; Young and Yang 2004; Yi et al. 2013).

Third, while our results clearly show a key contribution of GSK-3 signaling to DA-modulated excitability of interneurons which is consistent with altered GSK-3 signaling in the *Df(16)A*$^{+/-}$ mice (Tamura et al. 2016), contribution of other signaling pathways that mediate the effects of DA receptor activation, such as PKA signaling, cannot be excluded conclusively. Analysis of role of various signaling pathways in the excitability of pyramidal cells and interneurons and how they are affected by 22q11.2 deletions awaits further exploration in future studies.

Fourth, our model does not take into account the different subpopulations of PFC layer V pyramidal neurons, such as the recently described sag and non-sag neurons (Dembrow et al. 2010; Seong and Carter 2012; Shepherd 2013). Both types of neurons are detected in WT and *Df(16)A*$^{+/-}$ mice, but respond to D1R and D2R modulation similarly. This was true for the differences in both D2R and D1R modulation between WT and *Df(16)A*$^{+/-}$ mice, and therefore, this neuronal heterogeneity does not affect the interpretation of our findings. It remains possible that the effect on PFC layer V pyramidal neuron heterogeneity is age dependent. We performed all the experiments in adult mice (after postnatal day 58) whereas in the Seong and Carter (2012) study, experiments were conducted at postnatal day 28, before puberty. Possible age-dependent effects of neuronal heterogeneity can be addressed in future experiments.

Fifth, there are obvious limitations in extrapolating our findings from mouse to human brain, given the well-established species-specific differences in morphology and gene-expression patterns of various receptors and channels (Yue et al. 2014). Using the primate brain as a proxy, it has been shown, for example, that D2R stimulation increases rather than decreases the firing of dorso-lateral PFC pyramidal neurons (Wang et al. 2004; Ott et al. 2014; Puig and Miller 2015). Such differences may have an evolutionary basis but given the difficulties in attributing with certainty the layer origin of in vivo recordings in primate brains, they may also reflect brain area and layer-specific differences in dopaminergic modulation of pyramidal neuron firing. Indeed, in our study, we found that quinpirole increased the firing of layer II/III pyramidal neurons, an effect opposite to the one observed in layer V. Similarly, it has recently been shown that adrenergic modulation of synaptic transmission in the rat neocortex is brain area and layer-specific (Roychowdhury et al. 2014).

Despite these limitations, our work here unequivocally demonstrates an altered DA neuromodulation of PV+ inhibitory interneurons and unveils decreases in KCNQ-channel activity as a novel mechanism contributing to this abnormal DA responsiveness of interneurons, which emerges as a result of a SCZ-predisposing mutation. Moreover, our identification of a significant epistatic interaction between SNPs in *DRD2* and *KCNQ2* genes provides evidence for a more general role for KCNQ-channel activity and its dopaminergic modulation in association with general SCZ risk.

The Kv7/KCNQ/M family of potassium channels shows unusual biophysical properties: activation in the subthreshold range of membrane voltage, slow kinetics of activation and deactivation, and no inactivation (Brown and Adams 1980). The M current is widely present in the CNS and it is an important regulator of neuronal excitability and can be modulated by many different metabotropic receptors and neuromodulators (Delmas and Brown 2005; Lawrence et al. 2006; Cooper 2011). KCNQ channels are expressed in interneurons where they could specifically control interspike interval (Lawrence et al. 2006; Nieto-Gonzalez and Jensen 2013). Consistent with these findings, our work demonstrates that KCNQ2 is expressed in PV+ interneurons in the PFC and controls their firing. Furthermore, our findings show that activation of D2Rs in PV+ interneurons leads to KCNQ channels closure and increase in neuronal firing, likely via the GSK-3β signaling pathway. Thus, decreased KCNQ2 channel function results in inhibitory deficits from PV+ interneurons upon dopaminergic challenge. KCNQ2 is present in both excitatory neurons and interneurons. However, compared with that in the PV+ interneurons, we found much weaker expression of KCNQ2 in non-PV+ cells and little M-current in layer V pyramidal neurons. Moreover, we did not detect any significant genotypic difference in either KCNQ2 expression or function in pyramidal neurons. Thus our finding suggests that the 22q11.2 deletion leads to cell-type specific alterations in KCNQ2 expression and function. The mechanistic basis of this cell-type specificity remains to be determined. Potential mechanisms include cell-type specific alterations of transcription, splicing or protein stability all of which can in principle be mediated by genes removed by this genetic lesion (Karayiorgou et al. 2010; Fenelon et al. 2013). Along these lines, alternative splicing of the KCNQ2 gene generates several truncated variants that differ from native channels and exert a dominant-negative effect (Borsotto et al. 2007). It is conceivable that cell-type specific alterations in splicing resulting in altered ratios of fully functional to truncated forms may contribute to the observed decreases in M-type currents.

Intriguingly, while reduced KCNQ2 channel function in the PV+ interneurons in *Df(16)A*$^{+/-}$ mice renders these neurons less excitable upon D2R modulation, intrinsic PV+ excitability is not altered. This is likely due to either concomitant "protective" changes in gene expression or, more likely, homeostatic mechanisms (such as down-regulation of calcium channels) that may be sufficient to maintain PV+ interneuron excitability within a given dynamic range but may not tolerate the additional activity burden imposed by the dopaminergic challenge.

Notably, mutations in members of the KCNQ subfamily have been identified in human CNS diseases. Mutations in KCNQ2, KCNQ3, and KCNQ5 have been described in patients with epileptic disorder including early onset epileptic encephalopathies (Jentsch 2000; Kato et al. 2013; Milh et al. 2013) while recently deleterious KCNQ2 variants have been described in patients with autism (Jiang et al. 2013). Interestingly, common KCNQ2 variants have been associated with both SCZ and bipolar disorder (Borsotto et al. 2007; Judy et al. 2013; Lee et al. 2013). KCNQ2/3 channel openers are in development for the treatment of epilepsy (Kalappa et al. 2015), whereas KCNQ2/3 channel inhibitors were developed for treatment of learning and memory disorders (Wulff et al. 2009) as well as for age-related WM decline (Wang et al. 2011). Our discovery of altered

function of KCNQ2 as a consequence of the 22q11.2 deletion in the present study not only provides a new molecular and cellular mechanism for the pathophysiology but also a potential therapeutic drug target for SCZ.

Supplementary Material

Supplementary material is available at *Cerebral Cortex* online.

Funding

National Institute of Mental Health (R01MH097879 and R01MH096274 to J.A.G and R21MH090356 to H.Z).

Notes

We thank Dr Maria Karayiorgou for her help with generating the *Df(16)A*$^{+/-}$ mice, Dr K. Stark for providing experimental mice and Y. Sun and N. Haremaki for technical support and assistance with the mouse colony. We also thank Dr Manuel Covarrubias and Dr Ziyi Sun for critical reading of this manuscript. *Conflict of interest*: None declared.

References

Arguello PA, Gogos JA. 2010. Cognition in mouse models of schizophrenia susceptibility genes. Schizophr Bull. 36: 289–300.

Arguello PA, Gogos JA. 2011. Genetic and cognitive windows into circuit mechanisms of psychiatric disease. Trends Neurosci. 35:3–13.

Arnsten AF, Wang MJ, Paspalas CD. 2012. Neuromodulation of thought: flexibilities and vulnerabilities in prefrontal cortical network synapses. Neuron. 76:223–239.

Barch DM, Ceaser A. 2012. Cognition in schizophrenia: core psychological and neural mechanisms. Trends Cogn Sci. 16: 27–34.

Beaulieu JM, Gainetdinov RR, Caron MG. 2009. Akt/GSK3 signaling in the action of psychotropic drugs. Annu Rev Pharmacol Toxicol. 49:327–347.

Borsotto M, Cavarec L, Bouillot M, Romey G, Macciardi F, Delaye A, Nasroune M, Bastucci M, Sambucy JL, Luan JJ, et al. 2007. PP2A-Bgamma subunit and KCNQ2 K+ channels in bipolar disorder. Pharmacogenomics J. 7:123–132.

Brown DA, Adams PR. 1980. Muscarinic suppression of a novel voltage-sensitive K+ current in a vertebrate neurone. Nature. 283:673–676.

Brozoski TJ, Brown RM, Rosvold HE, Goldman PS. 1979. Cognitive deficit caused by regional depletion of dopamine in prefrontal cortex of rhesus monkey. Science. 205:929–932.

Chattopadhyaya B, Di Cristo G, Higashiyama H, Knott GW, Kuhlman SJ, Welker E, Huang ZJ. 2004. Experience and activity-dependent maturation of perisomatic GABAergic innervation in primary visual cortex during a postnatal critical period. J Neurosci. 24:9598–9611.

Chen L, Bohanick JD, Nishihara M, Seamans JK, Yang CR. 2007. Dopamine D1/5 receptor-mediated long-term potentiation of intrinsic excitability in rat prefrontal cortical neurons: Ca2+-dependent intracellular signaling. J Neurophysiol. 97: 2448–2464.

Cleghorn JM, Garnett ES, Nahmias C, Firnau G, Brown GM, Kaplan R, Szechtman H, Szechtman B. 1989. Increased frontal and reduced parietal glucose metabolism in acute untreated schizophrenia. Psychiatry Res. 28:119–133.

Consortium TSPG-WASG. 2011. Genome-wide association study identifies five new schizophrenia loci. Nat Genet. 43: 969–976.

Cooper EC. 2011. Made for "anchorin": Kv7.2/7.3 (KCNQ2/KCNQ3) channels and the modulation of neuronal excitability in vertebrate axons. Semin Cell Dev Biol. 22:185–192.

Crabtree GW, Gogos JA. 2014. Synaptic plasticity, neural circuits, and the emerging role of altered short-term information processing in schizophrenia. Front Synaptic Neurosci. 6:28.

Crabtree GW, Park AJ, Gordon JA, Gogos JA. 2016. Cytosolic accumulation of L-proline disrupts GABA-Ergic transmission through GAD blockade. Cell reports. 17:570–582.

Delmas P, Brown DA. 2005. Pathways modulating neural KCNQ/M (Kv7) potassium channels. Nat Rev Neurosci. 6:850–862.

Dembrow NC, Chitwood RA, Johnston D. 2010. Projection-specific neuromodulation of medial prefrontal cortex neurons. J Neurosci. 30:16922–16937.

Dong Y, White FJ. 2003. Dopamine D1-class receptors selectively modulate a slowly inactivating potassium current in rat medial prefrontal cortex pyramidal neurons. J Neurosci. 23:2686–2695.

Drew LJ, Crabtree GW, Markx S, Stark KL, Chaverneff F, Xu B, Mukai J, Fenelon K, Hsu PK, Gogos JA, et al. 2011. The 22q11.2 microdeletion: fifteen years of insights into the genetic and neural complexity of psychiatric disorders. Int J Dev Neurosci. 29:259–281.

Durstewitz D, Seamans JK. 2008. The dual-state theory of prefrontal cortex dopamine function with relevance to catechol-o-methyltransferase genotypes and schizophrenia. Biol Psychiatry. 64:739–749.

Ellegood J, Markx S, Lerch JP, Steadman PE, Genc C, Provenzano F, Kushner SA, Henkelman RM, Karayiorgou M, Gogos JA. 2014. Neuroanatomical phenotypes in a mouse model of the 22q11.2 microdeletion. Mol Psychiatry. 19:99–107.

Fenelon K, Mukai J, Xu B, Hsu PK, Drew LJ, Karayiorgou M, Fischbach GD, Macdermott AB, Gogos JA. 2011. Deficiency of Dgcr8, a gene disrupted by the 22q11.2 microdeletion, results in altered short-term plasticity in the prefrontal cortex. Proc Natl Acad Sci USA. 108:4447–4452.

Fenelon K, Xu B, Lai CS, Mukai J, Markx S, Stark KL, Hsu PK, Gan WB, Fischbach GD, Macdermott AB, et al. 2013. The pattern of cortical dysfunction in a mouse model of a schizophrenia-related microdeletion. J Neurosci. 33:14825–14839.

Gao WJ, Goldman-Rakic PS. 2003. Selective modulation of excitatory and inhibitory microcircuits by dopamine. Proc Natl Acad Sci USA. 100:2836–2841.

Goldman-Rakic PS, Muly ECIII, Williams GV. 2000. D(1) receptors in prefrontal cells and circuits. Brain Res Brain Res Rev. 31: 295–301.

Gruber AJ, Calhoon GG, Shusterman I, Schoenbaum G, Roesch MR, O'Donnell P. 2010. More is less: a disinhibited prefrontal cortex impairs cognitive flexibility. J Neurosci. 30:17102–17110.

Haider B, Duque A, Hasenstaub AR, McCormick DA. 2006. Neocortical network activity in vivo is generated through a dynamic balance of excitation and inhibition. J Neurosci. 26: 4535–4545.

Hoftman GD, Datta D, Lewis DA. 2016. Layer 3 excitatory and inhibitory circuitry in the prefrontal cortex: developmental trajectories and alterations in schizophrenia. Biol Psychiatry.

Hoshi N, Zhang JS, Omaki M, Takeuchi T, Yokoyama S, Wanaverbecq N, Langeberg LK, Yoneda Y, Scott JD, Brown DA, et al. 2003. AKAP150 signaling complex promotes suppression of the M-current by muscarinic agonists. Nat Neurosci. 6:564–571.

Jentsch TJ. 2000. Neuronal KCNQ potassium channels: physiology and role in disease. Nat Rev Neurosci. 1:21–30.

Ji Y, Yang F, Papaleo F, Wang HX, Gao WJ, Weinberger DR, Lu B. 2009. Role of dysbindin in dopamine receptor trafficking and cortical GABA function. Proc Natl Acad Sci USA. 106: 19593–19598.

Jiang YH, Yuen RK, Jin X, Wang M, Chen N, Wu X, Ju J, Mei J, Shi Y, He M, et al. 2013. Detection of clinically relevant genetic variants in autism spectrum disorder by whole-genome sequencing. Am J Hum Genet. 93:249–263.

Judy JT, Seifuddin F, Pirooznia M, Mahon PB, Jancic D, Goes FS, Schulze T, Cichon S, Noethen M, Rietschel M, et al. 2013. Converging evidence for epistasis between ANK3 and potassium channel Gene KCNQ2 in bipolar disorder. Front Genet. 4:87.

Kaenmaki M, Tammimaki A, Myohanen T, Pakarinen K, Amberg C, Karayiorgou M, Gogos JA, Mannisto PT. 2010. Quantitative role of COMT in dopamine clearance in the prefrontal cortex of freely moving mice. J Neurochem. 114:1745–1755.

Kalappa BI, Soh H, Duignan KM, Furuya T, Edwards S, Tzingounis AV, Tzounopoulos T. 2015. Potent KCNQ2/3-specific channel activator suppresses in vivo epileptic activity and prevents the development of tinnitus. J Neurosci. 35: 8829–8842.

Kapfhamer D, Berger KH, Hopf FW, Seif T, Kharazia V, Bonci A, Heberlein U. 2010. Protein Phosphatase 2a and glycogen synthase kinase 3 signaling modulate prepulse inhibition of the acoustic startle response by altering cortical M-Type potassium channel activity. J Neurosci. 30:8830–8840.

Karayiorgou M, Flint J, Gogos JA, Malenka RC. 2012. The best of times, the worst of times for psychiatric disease. Nat Neurosci. 15:811–812.

Karayiorgou M, Simon TJ, Gogos JA. 2010. 22q11.2 microdeletions: linking DNA structural variation to brain dysfunction and schizophrenia. Nat Rev Neurosci. 11:402–416.

Kato M, Yamagata T, Kubota M, Arai H, Yamashita S, Nakagawa T, Fujii T, Sugai K, Imai K, Uster T, et al. 2013. Clinical spectrum of early onset epileptic encephalopathies caused by KCNQ2 mutation. Epilepsia. 54:1282–1287.

Lawrence JJ, Saraga F, Churchill JF, Statland JM, Travis KE, Skinner FK, McBain CJ. 2006. Somatodendritic Kv7/KCNQ/M channels control interspike interval in hippocampal interneurons. J Neurosci. 26:12325–12338.

Lee YH, Kim JH, Song GG. 2013. Pathway analysis of a genome-wide association study in schizophrenia. Gene. 525:107–115.

Ljungstrom T, Grunnet M, Jensen BS, Olesen SP. 2003. Functional coupling between heterologously expressed dopamine D(2) receptors and KCNQ channels. Pflugers Arch. 446:684–694.

Manoach DS. 2003. Prefrontal cortex dysfunction during working memory performance in schizophrenia: reconciling discrepant findings. Schizophr Res. 60:285–298.

Marin O. 2012. Interneuron dysfunction in psychiatric disorders. Nat Rev Neurosci. 13:107–120.

Milh M, Boutry-Kryza N, Sutera-Sardo J, Mignot C, Auvin S, Lacoste C, Villeneuve N, Roubertie A, Heron B, Carneiro M, et al. 2013. Similar early characteristics but variable neurological outcome of patients with a de novo mutation of KCNQ2. Orphanet J Rare Dis. 8:80.

Mukai J, Tamura M, Fenelon K, Rosen AM, Spellman TJ, Kang R, MacDermott AB, Karayiorgou M, Gordon JA, Gogos JA. 2015. Molecular substrates of altered axonal growth and brain connectivity in a mouse model of schizophrenia. Neuron. 86:680–695.

Nagano-Saito A, Dagher A, Booij L, Gravel P, Welfeld K, Casey KF, Leyton M, Benkelfat C. 2013. Stress-induced dopamine release in human medial prefrontal cortex - F-Fallypride / PET study in healthy volunteers. Synapse. 67:821–830.

Nieto-Gonzalez JL, Jensen K. 2013. BDNF depresses excitability of parvalbumin-positive interneurons through an M-Like current in rat dentate gyrus. PLoS One. 8:e67318.

O'Donnell P. 2003. Dopamine gating of forebrain neural ensembles. Eur J Neurosci. 17:429–435.

Ott T, Jacob SN, Nieder A. 2014. Dopamine receptors differentially enhance rule coding in primate prefrontal cortex neurons. Neuron. 84:1317–1328.

Paterlini M, Zakharenko SS, Lai WS, Qin J, Zhang H, Mukai J, Westphal KG, Olivier B, Sulzer D, Pavlidis P, et al. 2005. Transcriptional and behavioral interaction between 22q11.2 orthologs modulates schizophrenia-related phenotypes in mice. Nat Neurosci. 8:1586–1594.

Paul K, Cox CL. 2013. Age-dependent actions of dopamine on inhibitory synaptic transmission in superficial layers of mouse prefrontal cortex. J Neurophysiol. 109:1323–1332.

Puig MV, Miller EK. 2015. Neural substrates of dopamine D2 receptor modulated executive functions in the monkey prefrontal cortex. Cereb Cortex. 25:2980–2987.

Richtand NM, Woods SC, Berger SP, Strakowski SM. 2001. D3 dopamine receptor, behavioral sensitization, and psychosis. Neurosci Biobehav Rev. 25:427–443.

Rodriguez-Murillo L, Gogos JA, Karayiorgou M. 2012. The genetic architecture of schizophrenia: new mutations and emerging paradigms. Annu Rev Med. 63:63–80.

Roychowdhury S, Zwierzchowski AN, Garcia-Oscos F, Olguin RC, Delgado RS, Atzori M. 2014. Layer- and area-specificity of the adrenergic modulation of synaptic transmission in the rat neocortex. Neurochem Res. 39:2377–2384.

Rudy B, Fishell G, Lee S, Hjerling-Leffler J. 2010. Three groups of interneurons account for nearly 100% of neocortical GABAergic neurons. Dev Neurobiol. 71:45–61.

Sanders SJ, He X, Willsey AJ, Ercan-Sencicek AG, Samocha KE, Cicek AE, Murtha MT, Bal VH, Bishop SL, Dong S, et al. 2015. Insights into autism spectrum disorder genomic architecture and biology from 71 risk loci. Neuron. 87:1215–1233.

Santana N, Mengod G, Artigas F. 2009. Quantitative analysis of the expression of dopamine D1 and D2 receptors in pyramidal and GABAergic neurons of the rat prefrontal cortex. Cereb Cortex. 19:849–860.

Santini E, Porter JT. 2010. M-type potassium channels modulate the intrinsic excitability of infralimbic neurons and regulate fear expression and extinction. J Neurosci. 30:12379–12386.

Schultz W. 2002. Getting formal with dopamine and reward. Neuron. 36:241–263.

Seong HJ, Carter AG. 2012. D1 receptor modulation of action potential firing in a subpopulation of layer 5 pyramidal neurons in the prefrontal cortex. J Neurosci. 32:10516–10521.

Sesack SR, Bunney BS. 1989. Pharmacological characterization of the receptor mediating electrophysiological responses to dopamine in the rat medial prefrontal cortex: a microiontophoretic study. J Pharmacol Exp Ther. 248:1323–1333.

Shepherd GM. 2013. Corticostriatal connectivity and its role in disease. Nat Rev Neurosci. 14:278–291.

Stark KL, Xu B, Bagchi A, Lai WS, Liu H, Hsu R, Wan X, Pavlidis P, Mills AA, Karayiorgou M, et al. 2008. Altered brain microRNA biogenesis contributes to phenotypic deficits in a 22q11-deletion mouse model. Nat Genet. 40:751–760.

Tamura M, Mukai J, Gordon JA, Gogos JA. 2016. Developmental Inhibition of Gsk3 Rescues Behavioral and Neurophysiological

Deficits in a Mouse Model of Schizophrenia Predisposition. Neuron. 89:1100–1109.

Tseng KY, Lewis BL, Hashimoto T, Sesack SR, Kloc M, Lewis DA, O'Donnell P. 2008. A neonatal ventral hippocampal lesion causes functional deficits in adult prefrontal cortical interneurons. J Neurosci. 28:12691–12699.

Tseng KY, O'Donnell P. 2004. Dopamine-glutamate interactions controlling prefrontal cortical pyramidal cell excitability involve multiple signaling mechanisms. J Neurosci. 24:5131–5139.

Vijayraghavan S, Wang M, Birnbaum SG, Williams GV, Arnsten AF. 2007. Inverted-U dopamine D1 receptor actions on prefrontal neurons engaged in working memory. Nat Neurosci. 10:376–384.

Wang HS, Pan Z, Shi W, Brown BS, Wymore RS, Cohen IS, Dixon JE, McKinnon D. 1998. KCNQ2 and KCNQ3 potassium channel subunits: molecular correlates of the M-channel. Science. 282:1890–1893.

Wang M, Gamo NJ, Yang Y, Jin LE, Wang XJ, Laubach M, Mazer JA, Lee D, Arnsten AF. 2011. Neuronal basis of age-related working memory decline. Nature. 476:210–213.

Wang M, Vijayraghavan S, Goldman-Rakic PS. 2004. Selective D2 receptor actions on the functional circuitry of working memory. Science. 303:853–856.

Weinberger DR, Berman KF. 1996. Prefrontal function in schizophrenia: confounds and controversies. Philos Trans R Soc Lond B Biol Sci. 351:1495–1503.

Weinberger DR, Berman KF, Zec RF. 1986. Physiologic dysfunction of dorsolateral prefrontal cortex in schizophrenia. I. Regional cerebral blood flow evidence. Arch Gen Psychiatry. 43:114–124.

Williams GV, Goldman-Rakic PS. 1995. Modulation of memory fields by dopamine D1 receptors in prefrontal cortex. Nature. 376:572–575.

Wulff H, Castle NA, Pardo LA. 2009. Voltage-gated potassium channels as therapeutic targets. Nat Rev Drug Discov. 8: 982–1001.

Xu B, Hsu PK, Stark KL, Karayiorgou M, Gogos JA. 2013. Derepression of a neuronal inhibitor due to miRNA dysregulation in a schizophrenia-related microdeletion. Cell. 152: 262–275.

Yi F, Zhang XH, Yang CR, Li BM. 2013. Contribution of dopamine d1/5 receptor modulation of post-spike/burst afterhyperpolarization to enhance neuronal excitability of layer v pyramidal neurons in prepubertal rat prefrontal cortex. PLoS One. 8:e71880.

Yizhar O, Fenno LE, Prigge M, Schneider F, Davidson TJ, O'Shea DJ, Sohal VS, Goshen I, Finkelstein J, Paz JT, et al. 2011. Neocortical excitation/inhibition balance in information processing and social dysfunction. Nature. 477: 171–178.

Young CE, Yang CR. 2004. Dopamine D1/D5 receptor modulates state-dependent switching of soma-dendritic Ca2+ potentials via differential protein kinase A and C activation in rat prefrontal cortical neurons. J Neurosci. 24:8–23.

Yue F, Cheng Y, Breschi A, Vierstra J, Wu W, Ryba T, Sandstrom R, Ma Z, Davis C, Pope BD, et al. 2014. A comparative encyclopedia of DNA elements in the mouse genome. Nature. 515:355–364.

Zhang Z, Jiao YY, Sun QQ. 2011. Developmental maturation of excitation and inhibition balance in principal neurons across four layers of somatosensory cortex. Neuroscience. 174:10–25.

Zhong P, Yan Z. 2014. Distinct physiological effects of dopamine D4 receptors on prefrontal cortical pyramidal neurons and fast-spiking interneurons. Cereb Cortex. 26:180–191.